UNIVERSITÀ
DI PAVIA

Dipartimento di Biologia e Biotecnologie "L. Spallanzani"

Laurea Magistralis in Neurobiology

Investigation of selected antipsychotic medications and their actions on $GABA_A$ receptors

Indagine su farmaci antipsicotici selezionati e sulla loro azione sui recettori $GABA_A$

Supervisor:
Prof. Marco Peviani

Co-supervisor:
Dr. Margot Ernst

Tesi Sperimentale di:
Virginia Novelli

Anno Accademico 2025/2026

INDEX

Abstract 1

Abstract (*Italian version*) 2

1. Introduction 3

1.1 Schizophrenia 3

1.1.1 Dopaminergic, glutamatergic, and GABAergic hypotheses ... 5

1.2 $GABA_A$ receptors 8

1.2.1 Subunits, their localisation, and pentameric arrangements 8

1.2.2 Selected $GABA_A$ receptor agonists and antagonists 14

1.2.3 $GABA_A$ receptor modulators 15

2. Aim of this study 20

3. Materials and methods 22

3.1 Radioligand displacement assays procedure 22

3.1.1 Preparation of rat hippocampal membranes 22

3.1.2 Preparation of the sample solutions 24

3.1.3 Preparation of the sample tubes 26

3.1.4 Filtration and counting 27

3.2 Computational analyses 27

3.2.1 Computational alignments 27

3.2.2 Computational docking 28

4. Results 30

4.1 Results of the radioligand displacement assay experiments 30

4.2 Results of the computational analyses 34

4.2.1 Computational alignments 34

4.2.2 Computational re-docking and docking 36

5. Discussion 54

5.1 Results of the radioligand displacement assays 54

5.2 Results of the computational analyses 54

5.3 Final considerations, limitations, conclusion 56

6. List of abbreviations 58

7. References 63

8. Supplementary materials 77

ABSTRACT

Schizophrenia is a complex psychiatric disorder whose aetiology involves genetic, environmental, and neurobiological factors, including alterations in the dopaminergic, glutamatergic, and GABAergic neurotransmitter systems. Indeed, an imbalance in excitation/inhibition (E/I) homeostasis plays a key role in the pathophysiology of the disorder. Hippocampal $GABA_A$ receptors, particularly those expressing the α5 subunit, represent an important pharmacological target for modulating neuronal activity and improving deficits associated with schizophrenia.

This study aimed to experimentally investigate the orthosteric binding of a series of selected antipsychotic drugs (asenapine, haloperidol, olanzapine, perphenazine, quetiapine, risperidone, and zuclopenthixol) to $GABA_A$ receptors, using loxapine as a control. The research was structured around an integrated approach:

1. Radioligand displacement assays: conducted on rat hippocampal membranes using [^{3}H]-muscimol as a tracer, to evaluate the compounds' ability to displace this $GABA_A$ receptor agonist from the receptors themselves, at concentrations of 1 mM and 100 µM.
2. Computational analyses: including observations of pharmacophore alignments with the VMD program, molecular docking studies performed with DiffDock, and interaction analyses carried out with PLIP. The focus was specifically on olanzapine and loxapine, using the PDB entry 6HUK.

The results of the displacement assays and computational analyses confirmed the orthosteric binding profile of loxapine. Olanzapine was identified as the only other compound capable of displaying consistent behaviour with reduction of muscimol binding, similar to that of the control loxapine, suggesting a potential orthosteric mechanism of action. Beyond the intrinsic methodological limitations of the *in vitro* assays and deep learning models employed for docking, this preliminary study provides insights into the pharmacological profile of antipsychotics on hippocampal $GABA_A$ receptors.

ABSTRACT (*Italian version*)

La schizofrenia è un disturbo psichiatrico complesso la cui eziologia coinvolge fattori genetici, ambientali e neurobiologici, tra cui alterazioni nei sistemi neurotrasmettitoriali dopaminergico, glutamatergico e GABAergico. Infatti, un disequilibrio nell'omeostasi eccitazione/inibizione (E/I) gioca un ruolo chiave nella patofisiologia del disturbo. I recettori $GABA_A$ ippocampali, in particolare quelli esprimenti la subunità α5, rappresentano un importante bersaglio farmacologico per modulare l'attività neuronale e migliorare i deficit associati alla schizofrenia.

Questo studio ha avuto come obiettivo l'investigazione sperimentale del legame ortosterico di una serie di farmaci antipsicotici selezionati (asenapina, aloperidolo, olanzapina, perfenazina, quetiapina, risperidone e zuclopentixolo) sui recettori $GABA_A$, usando la loxapina come controllo. La ricerca si è articolata in un approccio integrato:

1. Saggi di spiazzamento del radioligando: condotti su membrane ippocampali di ratto utilizzando [^{3}H]-muscimolo come tracciante, per valutare la capacità dei composti di spiazzare questo agonista dei recettori $GABA_A$ dai recettori stessi, a concentrazioni di 1 mM e 100 μM.
2. Analisi computazionali: inclusive di osservazione degli allineamenti di farmacofori mediante il programma VMD, studi di docking molecolare eseguiti con DiffDock e analisi di interazioni condotte con PLIP. L'attenzione si è concentrata in particolare su olanzapina e loxapina, utilizzando la voce PDB 6HUK.

I risultati dei saggi di spiazzamento e delle analisi computazionali hanno confermato il profilo di legame ortosterico della loxapina. L'olanzapina è stata identificata come l'unico altro composto in grado di mostrare un comportamento coerente con la riduzione del legame del muscimolo, simile a quello del controllo loxapina, suggerendo un potenziale meccanismo d'azione ortosterico. Al di là dei limiti metodologici intrinseci dei saggi in vitro e dei modelli di deep learning impiegati per il docking, questo studio preliminare offre indicazioni sul profilo farmacologico degli antipsicotici a livello dei recettori $GABA_A$ dell'ippocampo.

1. Introduction

1.1 Schizophrenia

Schizophrenia is a psychiatric disorder belonging to the spectrum of psychotic disorders (Zhan et al., 2023). It affects about 1% of the population worldwide, with a higher prevalence in males and a peak onset in the late teenage years or early adulthood (Zhan et al., 2023). It is characterised by positive, negative, and cognitive symptoms (Almulla et al., 2021). Positive symptoms reflect new and maladaptive mental processes and behaviours not present before the onset of the disorder (Almulla et al., 2021). They chiefly include hallucinations, delusions, and disorganised speech (Almulla et al., 2021). Negative symptoms mainly include poverty of content and form of thinking and impairment in emotional reactivity (Wójciak & Rybakowski, 2018). Ultimately, cognitive symptoms refer to issues with memory, reasoning, problem-solving, and processing speed (Carbon & Correll, 2014). These symptoms can have different levels of severity and a significant influence on the everyday life of the affected individual (Adamu et al., 2023).

The impairment in cognitive and executive functions is a hallmark of this disorder, and it is associated with abnormalities in the frontal lobe (Adamu et al., 2023). A reduction in grey matter is noted in the inferior frontal gyrus (IFG) and the middle frontal gyrus (MFG), which are both part of the prefrontal cortex, as well as in the anterior cingulate gyrus (Adamu et al., 2023). In particular, the subgenual cingulate - a portion of the anterior cingulate gyrus - might be associated with the affective blunting typical of this pathology (Glahn et al., 2008). Beyond these regions, similar alterations extend to the medial temporal lobe (including the amygdala, hippocampus, and parahippocampal gyrus) and regions of the superior temporal gyrus (Shenton et al., 2001). Specifically, the volume reduction in the hippocampus and parahippocampal gyrus could explain the memory deficits observed in patients (Shenton et al., 2001). On the other hand, fractional anisotropy (FA) reductions in the corona radiata, which contains reciprocal connections from the thalamus to the cerebral cortex, have been associated with auditory verbal hallucinations (Kelly et al., 2018). Lastly, the enlargement of the lateral ventricles and the increase in cerebrospinal fluid (CSF) volume cause

destabilised brain fluid dynamics and loss of brain tissue (Adamu et al., 2023). This could lead to the disruption of the thalamus, basal ganglia, and hypothalamus, and might therefore be associated with cognitive deficits and emotional dysregulation (Adamu et al., 2023).

These are the main anatomical changes that characterise this disease. Besides them, schizophrenia has a complex aetiology related to environmental, genetic, and neurobiological factors (Sohal, 2024). It is more common in individuals born in winter months, as there is a higher association with in utero exposure to maternal infections during the second trimester (Sohal, 2024). Even micronutrient deficiency during this developmental stage can represent a risk, particularly low levels of vitamin D (McGrath et al., 2010). Furthermore, this disorder has a heritability of ~60%-80% (Sohal, 2024). A recent genome-wide association study (GWAS) has identified common variant associations at 287 genetic loci, correlated with 120 genes (Sohal, 2024).

Individuals with 22q11.2 microdeletions might develop symptoms of schizophrenia. Three candidate genes are identified in this region: *PRODH*, *COMT*, and *ZDHHC8* (Purcell et al., 2014; Squarcione et al., 2013). Mutations in *PRODH* and *COMT* result in aberrant levels of GABA, glutamate, and dopamine, and of catecholamines, respectively, but their functionalities are not completely clear (Karam et al., 2010). *ZDHHC8* gene dysfunction causes alterations in hippocampal neurons, as well as both cognitive and behavioural deficits (Karam et al., 2010). Many of the other genetic loci associated with schizophrenia normally code for excitatory and inhibitory neurotransmission components, or proteins involved in the development of the correct excitation/inhibition (E/I) equilibrium (Howes & Shatalina, 2022). These genes code for constituents of NMDA, AMPA, and GRM3 glutamate receptors, as well as for elements of the postsynaptic protein scaffold of excitatory synapses involved in NMDAR-dependent control of AMPA receptor potentiation (Howes & Shatalina, 2022). The same applies to GABA receptors, as these genes also code for their structural components or proteins that mediate their turnover (Howes & Shatalina, 2022). Overall, most of the genes responsible for schizophrenia are expressed on excitatory glutamatergic neurons from the cerebral cortex and hippocampus, cortical inhibitory interneurons, and medium spiny neurons (Skene et al., 2018).

The receptors just mentioned represent the targets for the neurotransmitters glutamate and GABA. Neurotransmitter signalling is one of the key neurobiological factors connected to the aetiology of schizophrenia. In this regard, three main hypotheses account for the alterations within brain circuits in schizophrenia and the emergence of its symptoms: the dopaminergic, glutamatergic and GABAergic hypotheses (Sohal, 2024; Fujihara, 2023; Howes & Shatalina, 2022).

1.1.1 Dopaminergic, glutamatergic, and GABAergic hypotheses

Concerning dopamine, molecular imaging techniques have revealed significant elevations in striatal dopamine synthesis in schizophrenic patients (Brunelin et al., 2013). The excessive dopaminergic signalling is connected to psychotic symptoms and is the core of the dopaminergic hypothesis, which is grounded in two major observations (Howes & Shatalina, 2022; Frankle et al., 2018). The first states that drugs directly or indirectly increasing dopamine receptor activation exacerbate psychotic symptoms in schizophrenic patients, and can induce them in healthy individuals (Frankle et al., 2018). The second declares that all current antipsychotics block dopamine D2 receptors (D2Rs) (Howes & Kapur, 2009).

Moreover, aberrant D2R signalling may disrupt thalamocortical communication, and an excessive activation of these receptors in the striatum is sufficient to cause hallucinations and deficits in working memory (Sohal, 2024). Empirical data confirmed that D2R-blocking antipsychotics can provide minimal benefit for cognitive deficits (Sohal, 2024). Furthermore, continuous administration can lead to dopamine sensitivity, causing a reduction in antipsychotic efficacy after long-term exposure (Tiihonen et al., 2025). This is supported by evidence showing that, on the one hand, up to 70% of patients on long-term treatment have experienced psychotic symptoms during the follow-up (Tiihonen et al., 2025). On the other hand, patients with shorter treatment duration and lower dosages of antipsychotics have shown improved outcomes (Tiihonen et al., 2025).

As a whole, the imbalance of the brain dopamine system plays a crucial role in the development of this disorder, and distinct dopamine subsystems are involved across different brain regions in schizophrenia (Zhao et al., 2025). Beyond D2 receptors, D1 receptors (D1Rs) have also to be considered, as they offer a better explain for negative symptoms (Zhao et al., 2025). Indeed, these symptoms are tied to dysfunctions of the prefrontal cortex,

where D1Rs are located (Zhao et al., 2025). The latter are not the target of classical antipsychotics, which are usually antagonists of D2R, but treatments targeted to striatal D1Rs can be more efficient than the classical ones (Moya et al., 2023). In schizophrenia, there are abnormalities in cortical dopamine neurotransmission and in the expression of D1Rs (Abi-Dargham et al., 2022). They are particularly present in the prefrontal cortex, and for this reason they can mediate cognition. This area is also connected to regulations of functions such as working memory, motivation, planning, and social behaviour (Abi-Dargham et al., 2022). There are current therapeutic strategies with D1Rs agonists, but the optimal administration has to be determined (Abi-Dargham et al., 2022).

In conclusion to this, even though the dopaminergic hypothesis provides a crucial framework for understanding the emergence of positive and negative symptoms, it is not sufficient on its own to explain a complex disorder such as schizophrenia. In addition, neither typical nor atypical antipsychotics have been shown to be fully effective in addressing negative symptoms and cognitive impairments. Consequently, the glutamatergic and GABAergic hypotheses address key gaps left unresolved by the dopaminergic hypothesis (Okubo et al., 2024).

The glutamatergic hypothesis derives from the observation that NMDA receptor antagonists, such as phencyclidine (PCP) and ketamine, induce positive symptoms as well as cognitive deficits that closely resemble those observed in schizophrenia (Sohal, 2024). Although anti-NMDAR antibodies are characteristic of anti-NMDAR autoimmune encephalitis, they are also found in approximately 8% of individuals with schizophrenia. This finding is consistent with the NMDAR hypofunctionality detected in this disorder, as these antibodies promote the internalisation and downregulation of NMDARs (Okubo et al., 2024). In addition, NMDAR antagonists directly inhibit channel pore permeability, further contributing to receptor dysfunction (Okubo et al., 2024).

Evidence suggests that ketamine may preferentially block NMDARs on GABAergic interneurons, particularly those expressing somatostatin (SST) (Sohal, 2024). This hypothesis is supported by recordings of inhibitory postsynaptic currents, in which reduced SST interneuron activity was observed using a GABAergic Cre-driver mouse line (Adell, 2025). These inhibitory GABAergic interneurons modulate the activity of cortical and/or hippocampal pyramidal cells, and their dysfunctions can lead to cortical disinhibition and

circuit-level dysregulation, producing a hyperglutamatergic state (Adell, 2025). At this stage, glutamate levels increase and exert excitotoxic effects, potentially leading to white matter tissue loss. The consequence is that glutamate levels tend to decline in chronic stages (Liemburg et al., 2016). Additionally, electrophysiological studies have shown that aberrant brain rhythms and synchronisation are present from the onset of the disorder, in particular reduced gamma oscillations. Given that inhibitory interneurons expressing the parvalbumin (PV) protein play a critical role in generating gamma oscillations, the hypothesis is that their dysfunction could result in cognitive dysfunction and psychotic symptoms (Adell, 2025; Gonzalez-Burgos & Lewis, 2012).

Considering these observations, substantial evidence indicates that glutamate and GABA are involved in an abnormal cortical and hippocampal E/I balance, which results to be a central hallmark of schizophrenia. In the future, a deeper understanding of this imbalance may foster the development of new therapeutic strategies (Adell, 2025). At present, methodologies targeting NMDAR co-agonists, glycine transporter inhibitors, and glutamate transporter regulators have yielded inconsistent clinical outcomes. These results underscore the heterogeneity of schizophrenia and highlight the necessity for novel therapeutic targets (Fadgyas-Stanculete & Capatina, 2025).

The glutamatergic hypothesis outlined above is in correlation with the GABAergic hypothesis. Indeed, glutamate and GABA operate in close functional coordination, with key aspects of GABAergic dysfunction already touching upon the E/I balance previously mentioned. Deficits in GAD67, a marker for GABAergic neurons, in cortical regions including sensory, motor, and limbic areas represent another hallmark feature of schizophrenia (Lewis et al., 2012). This reduced expression is particularly prominent in the aforementioned PV neurons, which play a pivotal role in synchronising action potentials (Fujihara, 2023). Consequently, the reduction of GAD67 in these neurons is hypothesised to underlie the emergence of cognitive symptoms in the disorder (Fujihara, 2023). Further neuropathological observations include the decreased expression of SST, $GABA_A$ receptor $\alpha1$, $\alpha4$, $\beta3$, $\gamma2$, and δ subunits, GABA transporter (GAT-1), neuropeptide Y, and cholecystokinin (CCK) (Hashimoto et al., 2008). Given these findings, targeted restoration of the GABAergic system represents a promising therapeutic avenue, with current research extensively utilising GAD67 knockout and knockdown rodent models to recapitulate these

deficits (Fujihara, 2023).

These were the hypotheses that illustrate the primary neurotransmitter systems involved in the pathophysiology of schizophrenia. While current pharmacological treatments rely predominantly on dopamine receptors, some drugs can also target the central muscarinic M1/M4 receptors (Singh, 2022). For instance, Xanomeline/trospium chloride is a combination therapy which removes positive symptoms and improves the negative and cognitive symptoms (Singh, 2022). Xanomeline is a cholinergic agonist, and trospium chloride reduces its adverse effects (Singh, 2022). Additionally, metabotropic glutamate receptor (mGluR) agonists reverse PCP-induced hyperlocomotion, stereotypic movements and extracellular glutamate elevations in rodents, and can improve both positive and negative symptoms (Karam et al., 2010). Agonists of the α7 nicotinic acetylcholine receptor also represent a promising target, as their activation enhances cortical dopamine release and improves learning and attentional processes in rodents (Karam et al., 2010).
Finally, $GABA_A$ receptors constitute another crucial therapeutic target, and are the focus of this thesis - in particular, the α5-containing $GABA_A$ receptors, preferentially expressed in the hippocampus (Uliana et al., 2026; Xu & Wong, 2018; Gill & Grace, 2014).

1.2 $GABA_A$ receptors

1.2.1 Subunits, their localisation, and pentameric arrangements

$GABA_A$ receptors are pentameric, ligand-gated ion channels that mediate chiefly neuronal inhibition in the postnatal mammalian brain. There is evidence of excitatory action in prenatal mammalian brains, and excitatory action in certain compartments of the mammalian nervous system (Topchiy et al., 2024; Kim & Hibbs, 2021; Marty & Llano, 2005). They are targets of GABA, which is the main inhibitory neurotransmitter in the central nervous system (Roth & Draguhn, 2012). Its main function is to reduce neuronal excitability and to synchronize neuronal populations (Roth & Draguhn, 2012). These receptors are mainly permeable to chloride (Cl^-), but they also allow the passage of bicarbonate, formate, propionate, acetate, cyanide, and halides (Sallard et al., 2021).

In humans and other mammalian species, nineteen $GABA_A$ receptor subunit encoding genes have been identified. They code for six α, three β, three γ, three ρ, and one each of the δ, ε, π, and θ subunits (Mohamad et al., 2023; Puthenkalam et al., 2016). The majority of $GABA_A$ receptors are composed of two α, two β, and one γ subunits. The most widespread composition is α1β2γ2, arranged as γ2β2α1β2α1 counter clockwise around the centre (Zhou et al., 2025; Sigel & Ernst, 2018). Similar to γ2 subunits, δ subunits usually also form combinations with α and β subunits. The composition, stoichiometry, and arrangement of receptors that contain the ε and θ subunits are not so well-known yet (Puthenkalam et al., 2016; Ramerstorfer et al., 2011).

Individual subunits can be localised e.g. with immunohistochemistry or immunocytochemistry (Fritschy et al., 1998; Pirker et al., 2000), by which it was shown that there are widely expressed subunits in mammalian brain, as well as subunits with anatomically restricted expression, such as the α5 and α6 subunits (Pirker et al., 2000). The assembly into pentamers follows complex rules that are not yet fully understood (Sente et al., 2022). Representative pentameric arrangements are displayed in Figure 1.

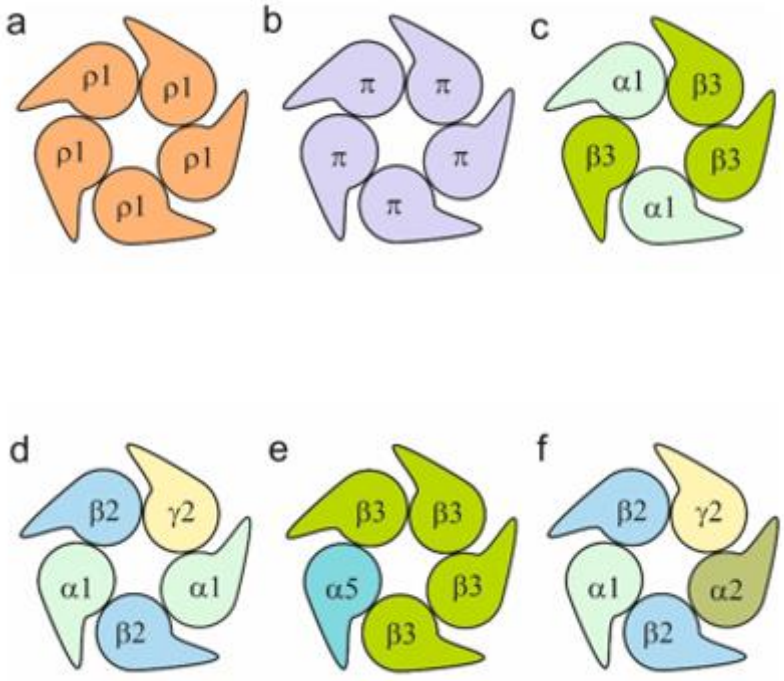

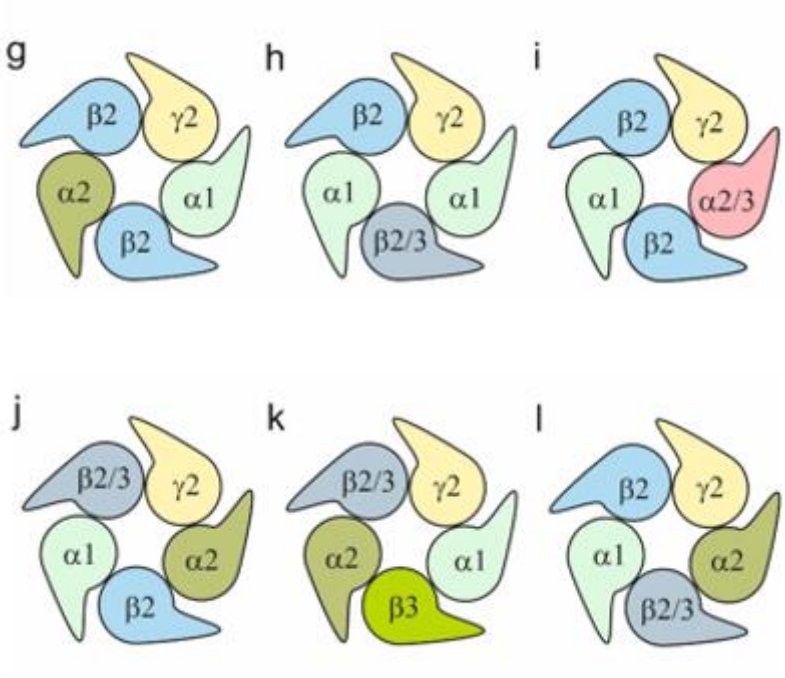

Figure 1. Representative known pentameric combinations with the α1, α2, α3, α5, β2, β3, and γ2 subunits, and also homopentamers. The drawings were created by the author of this thesis using the CorelDRAW software. Information about their existence is taken from the Zhou et al., 2025 paper and from the Protein Data Bank (PDB) platform (Vallat et al., 2026). The receptors are seen from the above, and each subunit has a distinctive colour. The point of each subunit represents the + side, while the opposite edge represents the – side.

Panel in Figure 2	Assembly	PDB ID
a	ρ1 × 5	8OQ6
b	π × 5	8VV0
c	α1β3	9FFU
d	α1β2γ2	9CRS
e	α5β3	6A96
f	α1α2β2γ2	9CT0
g	α1α2β2γ2	9CRV
h	α1β2β2/3γ2	9CXA
i	α1α2/3β2γ2	9CTP
j	α1α2β2β2/3γ2	9CSB
k	α1α2β2/3β3γ2	9CX7
l	α1α2β2β2/3γ2	9CTJ

Table 1. It shows the PDB ID of the illustrated pentamers in Figure 1. For figures h, i, j, k, and l, which have a double option for one of the subunits, only one PDB ID exists. This is because only one model was provided by the authors. The other one remains represented in Figure 1. Concerning the ρ subunit, only the PDB ID for ρ1 homopentamer is available. The reference papers found on the PDB page for the structures are listed below: a) Cowgill et al., 2023; b) Wang et al., 2025; c) Mihaylov et al., Forthcoming; d, f, g, h, i, j, k, l) Zhou et al., 2025; e) Liu et al., 2018.

The differences in the $GABA_A$ receptor composition of subunits are selectively adapted to the demands of specific neuronal types and circuits (Treviño et al., 2025). The brain deploys specific assemblies in strategic compartments to obtain a precise inhibitory control. From a general perspective, $GABA_A$ receptors are located in all brain regions (Treviño et al., 2025). They are not neuron-specific, but can be detected also in glial cells (Vélez-Fort et al., 2012).

In the human hippocampus, the structure relevant for this thesis, the subunits are distributed as follows: α1 and α3 are prominent in the dentate gyrus (DG), Cornu Ammonis 1 (CA1), and subiculum; α2 expression is strong in the DG and Cornu Ammonis 1 and 3 (CA3); α5 and γ2 are widespread; β2 and β3 are found in the DG, subiculum, and CA1 (Treviño et al., 2025; Stefanits et al., 2018). In rats, the same subunits and pentamers are detectable, with some differences in the distribution. (Treviño et al., 2025; Kerti-Szigeti & Nusser, 2016; Sperk et al., 1997). Pentamers c to l of Figure 1 may thus exist in the hippocampus, and additional arrangements such as α5β3γ2 that were not yet experimentally verified have been proposed. It is known from the literature that this pentamer exists, it is relevant from a pharmacological point of view, and it was used for the electrophysiological analyses conducted before this thesis (see Aim of the study chapter) (Sur et al., 1998). However, obtaining its stable recombinant complex with precise stoichiometry for cryo-EM structural determination is extremely complex. This is why it does not appear on the PDB and was not included in Figure 1.

Summarising, pentamers can consist of one to five different subunits, as shown in Figure 1. Moreover, the α1β3 receptor makes clear that there are also receptors without γ2 (Mortensen & Smart, 2006). Specific pentamers also occur in diverse peripheral tissues, but their function is still unknown (Bhandage et al., 2015). In particular, it is known that homopentamers made up by ρ subunits are located in the retina (Cutting et al., 1991), whereas the π subunits are observed particularly in tissues of the reproductive system

(Hedblom & Kirkness, 1997). Research is still ongoing, even for the rarest $GABA_A$ receptor subunits. Distinguishing between human and murine structures will be fundamental, along with understanding variability among individuals (Sequeira et al., 2019).

Different subunits determine different functional and pharmacological properties (Sun et al., 2023; Sieghart et al., 1999). Despite these dissimilarities, all $GABA_A$ receptor subunits exhibit a common structure: they include an N-terminal extracellular domain (ECD), four transmembrane domains (TMD) TM1-TM4, and a large intracellular "loop" (actually a domain, historically called loop) between TM3 and TM4 (Sieghart et al., 1999).
The subunits generally assemble in a pseudo-symmetrical way, where the contact interfaces are called principal or plus (+) side and complementary or minus (-) side. Binding pockets comprise two adjacent subunits, depending on whether they are +/- or -/+. These principal and complementary sides consist of seven loops in the ECD: loops A, B, and C from the principal subunit and loops D, E, F, and G from the complementary subunit (Mohamad et al., 2023; Puthenkalam et al., 2016). The organisation of the sides of the subunits leads to the formation of distinct binding sites: at the ECD β+/α interface, GABA binding sites are located (Figure 2b). These sites are also found at the ECD ρ+/ρ- interface, but they are bicuculline-sensitive only at the β+/α interface (Rosas-Arellano et al., 2023). Benzodiazepine (Bz) binding sites are located at the ECD α+/γ- interface (Figure 2b), whereas anaesthetics interact with distinct sites. In particular, etomidate (Eto) binds to the TMD β+/α- interface (Figure 2c). Barbiturates (Bbt) target sites at the TMD α+/β- and γ+/β- interfaces (Figure 2c). There is also a binding site for pyrazoloquinolinones (PQ), a class of synthetic allosteric modulators of $GABA_A$ receptors, which is located at the ECD α+/ β- interface, although PQ can also interact with the classic benzodiazepine site (Figure 2b). Finally, the channel blocker (ChB) site is the binding site for the $GABA_A$ receptor channel blockers. It is situated within the central pore of the receptor, where molecules physically obstruct the flux of Cl^- ions (Figure 2c) (Vega Alanis et al., 2020; Iorio et al., 2020).

In Figure 2, these binding sites are illustrated alongside a representation of a generic subunit interface. It is important to emphasise that these binding sites belong to the most widespread $GABA_A$ receptor composition, specifically the one with αβγ in a 2:2:1 ratio (Puthenkalam et al., 2016). For heteromeric receptors of alternative compositions, such as αβ or αβδ

combinations, the precise subunit arrangements have not been conclusively defined, and the exact number of physiological pentameric assemblies remains to be determined (Vega Alanis et al., 2020). Figure 2 was inserted to provide a comprehensive and complete mapping of the most well-characterised binding sites on these receptors, and therefore to give examples of representative ligands for each site. More details about pharmacology will be provided in the 1.2.3 subchapter.

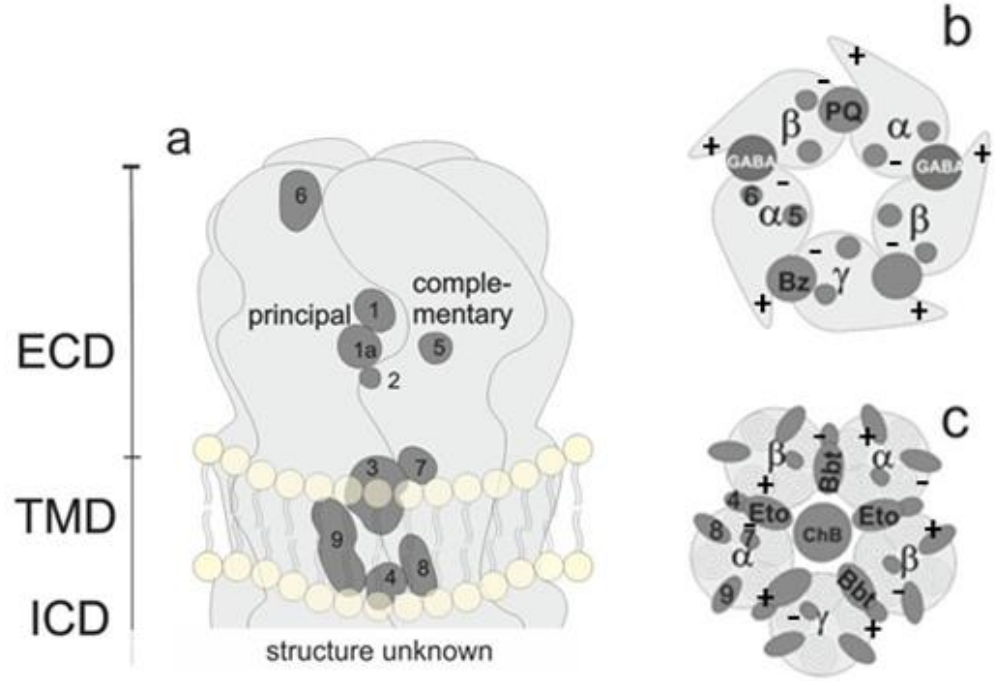

Figure 2. a) Representation of a generic subunit interface. Regions 1 and 1a form the ECD interface site, which harbours GABA or benzodiazepine sites. Region 2 is a cation site, while region 3 corresponds to the etomidate or barbiturate sites in the upper TMD. Region 4, at the lower TMD, is the site where positive modulatory steroids have been identified. Sites more remote to the interface, for which ligands are confirmed, include site 9 for negative modulatory steroids and tentative sites in positions 5,6,7,8. The structure of the intracellular domain (ICD) is unknown;
b) View of the ECD, seen from the above. GABA, Bz, and modulatory PQ sites are shown;
c) View of the TMD, seen from the above, of a canonical receptor, with Eto and Bbt sites shown explicitly. The ChB site is in the centre. Picrotoxin is an example of channel blocker (From Vega Alanis et al., 2020, license CC BY 4.0).
In both b) and c), the + and – symbols - indicating the principal and complementary sides, respectively - were added by the author of this thesis using PowerPoint 2013 and following information contained in the Iorio et al., 2020 paper.

$GABA_A$ receptors are particularly placed at postsynaptic sites, but they can also be found extrasynaptically. Receptors that include γ2 subunits in association with α1, α2, or α3

subunits are predominantly located postsynaptically. Receptors that contain α5 are predominantly extrasynaptic (Farrant & Nusser, 2005). Postsynaptic $GABA_A$ receptors have a phasic activity: they are notably adequate to generate precise, timed inhibitory postsynaptic potentials (IPSPs) that are the basis of inhibitory synaptic transmission (Sallard et al., 2021). On the other hand, the extrasynaptic $GABA_A$ receptors exhibit a tonic activity. They respond to low environmental GABA concentrations and generate persistent currents that modulate neuronal excitability (Sallard et al., 2021).

1.2.2 Selected $GABA_A$ receptor agonists and antagonists

In this subchapter, brief information about bicuculline and muscimol is provided. They act as an antagonist and an agonist of $GABA_A$ receptors, respectively, and they played a role in the work that was done for this thesis.

Muscimol, a psychoactive alkaloid isolated from the mushroom Amanita muscaria, is an agonist of $GABA_A$ receptors (Johnston, 2014). It binds to orthosteric GABA binding sites (Johnston, 2014) and exerts a powerful GABA-like activity on neurons (Müller et al., 2024). It is used in its tritiated form [^{3}H]-muscimol to study $GABA_A$ receptor subtypes (Rivera Illanes & Recabarren-Gajardo, 2024). In this thesis, [^{3}H]-muscimol was used as a tracer in the radioligand displacement assays.

a) b)

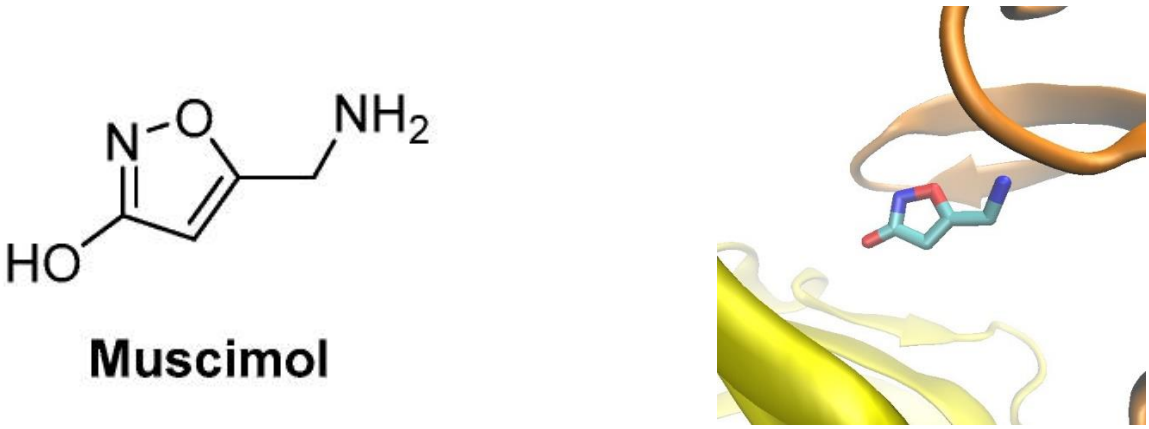

Figure 3. a) Muscimol chemical structure (from Vega Alanis et al., 2020, license CC BY 4.0); b) Muscimol structure visualised using the VMD software. It is visualised in cyan sticks, and

positioned between chain B (ρ1 subunit, in yellow) and chain A (ρ1 subunit, in orange). The structure of reference is the 9G60 (reference paper to be published), taken from the PDB. The red portions of the ligand represent oxygen atoms, while the blue portions represent the nitrogen atoms of the molecule.

As opposed to muscimol, bicuculline is a convulsing alkaloid that continues to be studied even forty years after the discovery of its effects on the $GABA_A$ receptors (Johnston, 2013), and it acts as a competitive antagonist at these receptors (Johnston, 2013). It is present in the 6HUK PDB structure (Masiulis et al., 2019) that was used for the computational analyses of this thesis. It was useful to individuate the GABA binding site that was utilised to test the molecular docking of some antipsychotics.

a) b)



Figure 4. a) Bicuculline chemical structure (from Vega Alanis et al., 2020, license C BY 4.0).
b) Bicuculline structure visualized using the VMD software. It is visualized in cyan sticks, and positioned between chain E (β3 subunit, in green) and chain D (α1 subunit, in purple). The structure of reference is the 6HUK, taken from the PDB. The red portions of the ligand represent oxygen atoms, while the blue portions represent the nitrogen atom of the molecule.

1.2.3 $GABA_A$ receptor modulators

$GABA_A$ receptors show one of the richest pharmacology of any therapeutic drug target, including agonists, antagonists, silent allosteric modulators (SAMs), and positive and negative allosteric modulators (PAMs and NAMs) (Thompson, 2024). Allosteric modulators require the presence of the endogenous ligand to exert their effects, and they bind to allosteric

sites, or rather sites different from the ones where the endogenous ligand binds. They modulate the GABA-elicited channel response (Vega Alanis et al., 2020). PAMs enhance the effect of the endogenous ligand, while NAMs diminish its effect. SAMs do not influence the effects of the endogenous ligand, but they can compete with a PAM or a NAM for the occupation of a binding site (Vega Alanis et al., 2020). On the other side, orthosteric antagonists attenuate or block the effect of an agonist. The difference with a NAM is that the orthosteric antagonist exerts its effects not in an allosteric site, but in the orthosteric site, where the endogenous ligand binds (Vega Alanis et al., 2020). Allosteric agonist- like effects are also known, sometimes also called GABA mimetic effects. This refers to the ability of compounds to open the channel in the absence of GABA by binding at allosteric sites, for example by some barbiturates (Pistis et al., 1999).
This is the general statement. Some features of the main α5-containing $GABA_A$ receptors modulators will now be addressed, providing examples for PAMs, SAMs, and NAMs.

Focusing first on PAMs, the majority of the benzodiazepines fall into this category. As already mentioned in the 1.2.1 subchapter, their classical binding site is located at the extracellular α+/γ- interface (Sigel & Ernst, 2018). They target $GABA_A$ receptors containing the α1, α2, α3, or α5 subunit non-selectively, each related to specific effects (Rudolph & Knoflach, 2011). Benzodiazepines exert sedative, hypnotic, muscle-relaxant, anxiolytic, and anticonvulsive effects. They are also being investigated for cognitive enhancement, pain relief, and depression (Sigel & Ernst, 2018). In addition, they can also be used in the treatment of epileptic attacks (Sanabria et al., 2021) and for pre-anaesthesia (Gaulton et al., 2021).

Functions	Drugs	ATC code
Anxiolytics	Diazepam	N05BA01
	Lorazepam	N05BA06
	Alprazolam	N05BA12
	Delorazepam	N05BA
	Bromazepam	N05BA08
Sedatives	Midazolam	N05CD08
	Lormetazepam	N05CD06
	Triazolam	N05CD05
	Brotizolam	N05CD09
	Flurazepam	N05CD01
Antiepileptics	Clonazepam	N03AE01

Table 2. Table with three of the main benzodiazepine functions in the first column. In the second column, there are the corresponding and most used benzodiazepines in Italy in 2024. Information is taken from the 2024 AIFA document. It is possible to find these drugs in that document looking for the equivalent code, which is written in the third column. For bromazepam, lormetazepam, triazolam, brotizolam, flurazepam, and clonazepam it is necessary to look for their name. For completeness, their codes were found in the DrugCentral database. N05B is the code for anxiolytics, N05C for hypnotics and sedatives, and N03A for antiepileptics (ATC/DDD Index, 2026).

The purpose of Table 2 is to summarise the main functions of benzodiazepines. Representative, commonly prescribed compounds for each category were selected from the Italian pharmaceutical context, as this work will be presented within an Italian academic institution. Consequently, this selection serves as a representative framework. Data from 2024 were chosen because complete datasets for 2025 were not yet available at the time of writing. Compounds were categorised in Table 2 according to their primary action. These data indicate that benzodiazepines are predominantly prescribed as anxiolytics and sedatives (AIFA, 2024, pages 277, 279, 299). Despite their large use, at least in Italy, benzodiazepines exhibit medical complications. They induce memory impairment, increase the risk of overdose, and lead to severe withdrawal symptoms (Fluyau et al., 2018).

In mice, it was demonstrated that the $GABA_A$ receptor α5 subunit mediates muscle-relaxant, but not sedative effects. The specificity is attributable to its localisation on motor neurons and within the dorsal horn of the spinal cord, as revealed through diazepam administration in genetically modified knock-in mice (Crestani et al., 2002).

Flumazenil is primarily classified as a SAM (Zhu et al., 2022). In rats, displacement assay experiments have demonstrated that this compound binds non-selectively to the benzodiazepine binding site across α1, α2, α3, and α5 subunits (Li et al., 2001).
It is clinically established to effectively reverse the signs and symptoms of benzodiazepine overdose (Spivey et al., 1993). Furthermore, in preclinical studies in rats, flumazenil has been shown to improve cognitive deficits following traumatic brain injury (TBI), a condition characterised by altered GABAergic transmission. However, only high doses enhanced cognitive performance in the Morris Water Maze (MWM), whereas low doses did not display any effect. These findings suggest that marked, dose-dependent receptor modulation is required to obtain cognitive improvements (Ochalski et al., 2010).
In addition, clinical pharmacovigilance data show a significant association between flumazenil and neurological adverse reactions. The main risks include seizures and withdrawal syndrome, particularly in benzodiazepine-dependent individuals. These findings were acquired using the FDA Adverse Event Reporting System (FAERS) database - which, however, has some limitations, such as duplicate and incomplete data (An & Jiang, 2025).

In contrast, basmisanil is a highly selective NAM targeting α5-containing $GABA_A$ receptors (Hipp et al., 2021). Overall, α5-selective NAMs have been extensively investigated for the potential development of cognitive-enhancing drugs (Jacob, 2019). In preclinical evaluations, these compounds - unlike non-selective α NAMs - do not exhibit pro-convulsant activity, whilst demonstrating favourable oral bioavailability and efficient blood-brain barrier (BBB) penetration (Jacob, 2019).
In humans, direct target engagement of basmisanil with α5 subunits was confirmed using positron emission tomography (PET), showing particularly high efficiency (Hipp et al., 2021). Furthermore, preclinical evidence indicates that modulation of α5-containing $GABA_A$ receptors with this drug enhances neuronal activity and molecular plasticity within the hippocampus (Daher et al., 2026). A phase 2b clinical trial evaluated basmisanil as a treatment for cognitive impairment associated with schizophrenia (CIAS) (Umbricht et al., 2026). Although the drug exhibited a promising pharmacological profile and good tolerability, it failed to demonstrate significant cognitive improvements in patients with schizophrenia (Umbricht et al., 2026). Nevertheless, current clinical evidence suggests that selective modulators represent significant models for the development of future targeted

drugs (Umbricht et al., 2026).

Overall, in schizophrenia, the $GABA_A$ receptor α5 subunit is significantly less available in the hippocampus of antipsychotic-free patients, and this may drive excessive excitation (Marques et al., 2021). Indeed, in rodents, the ventral hippocampus (vHipp) regulates dopamine signalling through a polysynaptic pathway projecting from the nucleus accumbens (NAc) to the ventral pallidum (VP), and ultimately to dopamine neurons in the ventral tegmental area (VTA) (Donegan et al., 2019). It has been demonstrated that hyperactivity within the vHipp-NAc pathway increases dopamine population activity in the VTA (Donegan et al., 2019). In this context, PAMs may attenuate this hyperdopaminergic state by selectively dampening dopamine activity within the central and lateral regions of the VTA (Uliana et al., 2026).

However, some antipsychotic compounds (ATC code: N05A; ATC/DDD Index 2026) display a NAM-like action, some acting allosterically, and some actually being orthosteric antagonists, and for most, the binding sites not being clear (Bampali et al., 2022). Negative modulation of α5-containing $GABA_A$ receptors has been shown to promote hippocampal gamma oscillations and long-term potentiation (Bampali et al., 2022).
Additional antipsychotics have been analysed in this thesis. The most significant reference papers for this work are Bampali et al., 2022 and Müller et al., 2024. In Bampali et al., 2022, it was demonstrated that loxapine, clozapine and chlorpromazine – three antipsychotics - reduced GABA-elicited currents in recombinant α5β3γ2 $GABA_A$ receptors. An orthosteric action mechanism for loxapine and clozapine, and an allosteric mechanism for chlorpromazine were suggested by radioligand displacement assay experiments. These were performed on rat hippocampal membranes, rich in α5 subunits, using [^{3}H]-muscimol as a tracer.

In Müller et al., 2024, radioligand displacement assays on rat hippocampal membranes confirmed an orthosteric action mechanism for loxapine and clozapine. For further investigation, computational docking analyses were conducted. It was observed that loxapine can occupy the same bicuculline binding site in the 6HUK structure, and thus the GABA binding site.

2. Aim of this study

The work described in this thesis was carried out in Vienna, at the Centre for Brain Research (Medical University of Vienna). The aim of this study is to specifically test orthosteric binding of selected antipsychotic medications on $GABA_A$ receptors. Asenapine, haloperidol, olanzapine, perphenazine, quetiapine, risperidone, and zuclopenthixol were the compounds investigated. They belong to different subclasses of antipsychotics (Leucht et al., 2024), and their choice was suggested by a psychiatrist who collaborates with the hosting laboratory. Electrophysiological studies were firstly conducted by the hosting laboratory in recombinant α5-containing $GABA_A$ receptors in HEK cells. The detected impact on the current by 100 µM compounds is summarised in Table 3, and reported alongside other findings as an Application Report (Sophion report, 2024).

Compound (100 µM)	% (residual) GABA response current (EC_{50})
GABA EC_{50} (6.9 µM)	96
Risperidone	28
Olanzapine	2
Asenapine	0
Zuclopenthixol	14
Loxapine	0
Haloperidol	89
Clozapine	2
Quetiapine	55
Perphenazine	6

Table 3. Results of the unpublished electrophysiological analyses conducted before the pilot studies of this thesis by the hosting laboratory. The left column shows the compounds used, and the currents elicited by GABA EC50, which was used as the reference current. In the right column, the % residual chloride currents induced by activation of the $GABA_A$ receptors without and with compound are shown. Higher values indicate that the compound did not reduce the current much. Conversely, lower

values mean that the compound strongly reduced it. Values near the 0 indicate complete suppression.

Clozapine was included in Table 3 for completeness, but was not re-tested in this thesis (Bampali et al., 2022; Müller et al., 2024). The other compounds in Table 3, which all reduced GABA currents, were tested in pilot muscimol displacement assays, and, for all of them, a pharmacophore model was generated by a collaboration partner. In the assays, the compounds were tested at the final concentrations of 1 mM and 100 µM (starting from 100 mM and 10 mM stock solutions, respectively). The first concentration was chosen because it was observed that saturation occurred at it in Müller et al., 2024. The second one was used because it was the concentration used in the electrophysiological study.
The compounds that displaced muscimol were then examined with a computational docking study to generate structural hypotheses for the observed displacement, and to support the orthosteric hypothesis.

Declaration: the author of this thesis performed a radioligand displacement assay study, which was designed as a preliminary, exploratory screening. Consequently, statistical evaluations were not possible. Moreover, she only visualised the best computational alignment results obtained, while she personally performed the docking studies, where the 6HUK PDB structure was used to match the previous work (Müller et al., 2024). Loxapine was used as a control in both radioligand displacement assays and computational alignments, since some information is already available from the Bampali et al., 2022 and Müller et al., 2024 papers. All Figures were made by the author, except where stated otherwise. Software used to generate them is provided in the Materials and methods chapter.

3. Materials and methods

3.1 Radioligand displacement assays procedure

3.1.1 Preparation of rat hippocampal membranes

Rat hippocampal membranes used for the radioligand displacement assays were prepared from thirty-six rat hippocampi, obtained from 3-, 4-, 5-, 7-week-old rats of both sexes. The solutions required for membrane preparation are listed in Table 4.

SOLUTION	COMPOSITION
500 mM Hepes	• 11.9 g Hepes / 100 mL, pH = 7.5 (NaOH, ca 19 mL 1 N); ➢ filter sterilisation, store at 4°C
TC500	• 500 mM Tris (MW 121.14): 60.6 g; • 155 mM citric acid (MW 210.14): 32.5 g; ➢ all in H2O to 1 L, pH = 7.1
Homogenisation Buffer	• 10 mM Hepes: 250 µL, 500 mM, pH = 7.5; • 1 mM EDTA: 50 µL (0.5 M); • 300 mM Sucrose: 2.5 g; • ¼ Complete Protease Inhibitor Tablette (Roche): ca 15 mg; ➢ all in Milli-Q water to 25 mL, set pH = 7.5
Wash Buffer	• 10 mM Hepes: 1 mL, 500 mM, pH = 7.5; • 1 mM EDTA: 100 µL (0.5 M): • ½ Complete Protease Inhibitor Tablette (Roche), ca 30 mg; ➢ All in Milli-Q water to 50 mL, set pH = 7.5
TC50	• 50 mL TC500; ➢ In H2O to 500 mL

50 mM Tris-Citrat + 150 mM NaCl (TC50/NaCl)	• 50 mL TC500; • 37.5 mL 2M NaCl; ➢ For 500 mL

Table 4. Solutions and corresponding compositions used for the preparation of rat hippocampal membranes.

- The Homogenisation Buffer was prepared by combining 250 µL of HEPES, 50 µL of EDTA, 2.5 g of sucrose, and one-quarter (15 mg) of a Complete Protease Inhibitor tablet (Roche). The solution was brought to 25 mL with Milli-Q water and adjusted to pH 7.5.

- The Wash Buffer was prepared by combining 1 mL of HEPES, 100 µL of EDTA, and half (30 mg) of a Complete Protease Inhibitor tablet (Roche). The solution was brought to 50 mL with Milli-Q water and adjusted to pH 7.5.

Both buffers were stored overnight at 4 °C before use. The following day, the thirty-six frozen hippocampi (~1.5 g total tissue) were thawed and divided equally into two SS34 centrifuge tubes (eighteen hippocampi per tube). Each tube was supplemented with 10 mL of Homogenisation Buffer, and tissue disruption was performed using an Ultra-Turrax homogeniser. The homogenates were balanced and centrifuged (20,000 rpm, 30 min, 4 °C). The resulting supernatants were discarded, and the pellets were retained. Each pellet was suspended in 10 mL of Wash Buffer and incubated on ice for 30 min. After homogenisation with the Ultra-Turrax, the tubes were balanced and centrifuged (20,000 rpm, 30 min, 4 °C). This washing step was repeated once more with 10 mL of Wash Buffer, omitting the ice incubation step. The final pellets were then stored overnight at -80 °C.

To remove endogenous GABA, membrane washing cycles were performed the following day. Pellets were thawed and suspended in 10 mL of TC50 buffer per SS34 tube, and then homogenised, balanced and centrifuged (20,000 rpm, 30 min, 4 °C). This washing procedure was repeated for two additional cycles. The resulting membrane pellets from both tubes were then pooled in a Falcon tube containing 6 mL of TC50 buffer. The suspension was then

aliquoted into four 1.5 mL Eppendorf tubes, each containing material equivalent to nine hippocampi. The samples were then centrifuged in an Eppendorf centrifuge (maximum speed, 30 min, 4 °C). The supernatants were discarded, and the membrane pellets were frozen in liquid nitrogen and stored at -80 °C.

3.1.2 Preparation of the sample solutions

Four pilot radioligand displacement assay experiments were performed, each by using one previously prepared Eppendorf aliquot. Each assay included membranes, drugs, GABA, TC50/NaCl buffer, DMSO, and [^{3}H]muscimol. Detailed pipetting schemes are provided in the Supplementary materials (Tables 11, 12, 13, 14). Instructions for the preparation of the solutions used are provided below. All materials were obtained from commercial suppliers, mostly Sigma-Aldrich.

- GABA: fresh GABA stock solution (100 mM) was prepared daily by weighing approximately 2 mg of GABA into an Eppendorf tube. The GABA obtained was dissolved in the corresponding TC50/NaCl volume, calculated using a conversion factor of 100 µL per milligram.

- Drugs: two stock solutions (100 mM and 10 mM) were prepared. For the 100 mM stock solution, approximately 3 mg of loxapine and 2 mg of the other antipsychotics were weighed inside Eppendorf tubes. For the 10 mM stock solution, a weight between 1 mg and 2 mg was required for each drug except loxapine, which was not used at this stock concentration. All the compounds were dissolved in the corresponding DMSO volume, calculated using Formula 1. The molecular weight of each drug, required in Formula 1, is reported in Table 5. Two additional 10 mM stock solutions were prepared for haloperidol and olanzapine in the fourth assay. The first, indicated as 10 mM#1 in Table 14 (Supplementary materials), was prepared by diluting 5 µL of their existing 100 mM stock in 45 µL of DMSO. The second one, indicated as 10 mM#2 in Table 14, was directly taken from their previously prepared 10 mM stock solution.

- [^{3}H]-muscimol: [^{3}H]-muscimol working solution was prepared fresh daily by diluting the [^{3}H]-muscimol stock (specific radioactivity of 26 Ci/mmol, concentration of 38.5 μM) in the corresponding TC50/NaCl buffer volume. This volume was calculated by multiplying the tube count by the pipetting scheme volume (40 μL), and then slightly rounded for operational standardisation. The starting [^{3}H]-muscimol volume to be taken from the stock, and to be diluted in TC50/NaCl inside an Eppendorf tube, was calculated using Formula 2, and solutions around 100 nM were obtained. This value was verified before each experiment, by checking the radioactivity of 5 μL of the resulting [^{3}H]-muscimol working solution in the beta-counter and by adding 2 mL of Rotiszint HighCapacity cocktail to it (expected values: 58 dpm/fmol and 29,000 dpm). The dpm values obtained were inserted in the online GraphPad Radioactivity Calculator to be converted into the corresponding concentration, and were compared with the theoretical 100 nM value.

- Membranes: a frozen aliquot of the hippocampal membranes was thawed before starting each experiment and homogenised with the Ultra-Turrax, while suspended in the corresponding TC50/NaCl volume inside a Falcon tube. This volume was obtained by multiplying the tube count by the pipetting scheme volume (320 μL), and then slightly rounded for operational standardisation.

$$V = \frac{m}{M \times MW}$$

Formula 1. Formula used to calculate the DMSO volume required for each of the drugs weighed. V is the volume to be found (in L, then converted in μL), m is the mass of each antipsychotic (g), M is the molarity (mol/L, corresponding to the 100 mM or 10 mM starting concentrations), and MW is the molecular weight of each antipsychotic (g/mol, Table 5).

Drug	Molecular weight (g/mol)
Asenapine	285.77
Haloperidol	375.86
Loxapine	327.808
Olanzapine	312.4
Perphenazine	403.97
Quetiapine	383.51
Risperidone	410.49
Zuclopenthixol	400.965

Table 5. Molecular weight of each used antipsychotic, found in several databases: Sigma-Aldrich, PubChem, Fisher Scientific, and BioGRID.

$$V1 = \frac{C2 \times V2}{C1}$$

Formula 2. Formula used to calculate the starting [^{3}H]-muscimol volume used for the preparation of its working solution. V1 is the starting [^{3}H]-muscimol volume, while V2 corresponds to the TC50/NaCl volume. C1 and C2 are 38.5 µM and 100 nM, respectively.

3.1.3 Preparation of the sample tubes

Each of the four assays was performed under distinct experimental conditions, meaning that not all drugs were tested in each experiment. All assays were performed in triplicate, with three tubes per experimental condition (100% control, GABA, drugs). Each tube contained a final volume of approximately 400 µL. The final dilutions within this volume were as follows: 1:10 for TC50/NaCl, GABA, and [^{3}H]-muscimol, and 1:100 for DMSO and drugs. The pipetting schemes (Supplementary materials, Tables 11, 12, 13, 14) specify the volumes of membranes, [^{3}H]-muscimol, and drug solutions, and even the volumes of TC50/NaCl buffer and DMSO solvent required for each tube.

3.1.4 Filtration and counting

After preparation of the tubes, the samples were incubated for 60 min at 4 °C. Subsequently, they were filtered through Whatman GF/B filters, which were rapidly washed three times with TC50 using a filtration apparatus. The filters retained the membrane-bound radioligand, whereas unbound ligand and residual assay components were removed during filtration and washing. The use of a cold TC50 buffer minimised nonspecific binding and reduced background signal. Following filtration, 2 mL of Rotiszint liquid scintillation cocktail were added to each filter, and the vials were placed in the beta-counter for radioactivity measurement. The obtained data were analysed and plotted using GraphPad Prism 8. Formula 3 was used to generate the corresponding graphs (Figure 5b and Figure 6b of the Results chapter).

$$\% \text{ binding} = \left(\frac{drug\ dpm - mean\ bk}{mean\ 100\% - mean\ bk}\right) \times 100$$

Formula 3. This formula was used to express each drug with respect to the control in Figure 5b and Figure 6b of the Results chapter. The control is fixed at 100%.

3.2 Computational analyses

3.2.1 Computational alignments

Computational alignment results were visualised using the VMD (Visual Molecular Dynamics; Humphrey et al., 1996) software. Asenapine, olanzapine, quetiapine, and zuclopenthixol obtained the best alignment with loxapine, and were observed super imposed on loxapine structure.

- Ligand visualisation: the five compounds were uploaded as mol2 files, which were made available by the collaborator of the hosting laboratory who performed the pharmacophore alignments.

3.2.2 Computational docking

Computational docking analyses were performed for bicuculline, loxapine, and olanzapine. Firstly, the DiffDock (Diffusion-based Molecular Docking) tool available on the NVIDIA platform (Corso et al., 2023) was utilised. The selected poses from DiffDock were then visualised on VMD, together with the experimental structure in the case of bicuculline, and their interaction profiles with the receptor were analysed using PLIP (Protein-Ligand Interaction Profiler) (Schake et al., 2025).

- Protein preparation: 6HUK was used for docking. The binding sites of interest were at two sides, A/B (α1/β3) and D/E (α1/β3) (β+/α- interface in both cases). Both were used and tested to re-dock bicuculline. The two dimers were saved in PDB format without bicuculline present, using the PDB-Tools platform (Jiménez-García et al., 2021), and used as input. They were merged with the selected poses and the experimental bicuculline for the PLIP platform, using SciMiner. For loxapine and olanzapine, the A/B site was used, and the same procedure was repeated.

- Ligand preparation: ligands were supplied to the docking program as mol2 files, and converted to sdf for SciMiner using ScienceCodons. Loxapine and olanzapine files were the same used in the computational alignment, while bicuculline atomic coordinates were taken from 6HUK and saved separately as an sdf file, converted to mol2 for VMD using ScienceCodons. All ligands are displayed as backbone structures without hydrogens.

- DiffDock: three different online platforms were explored for it: NVIDIA, Genophore, and UseGalaxy. NVIDIA was selected for its superior efficiency, overcoming Genophore's upload limitations and UseGalaxy's poor ligand representations. It generated poses with a default setting of twenty per run. For both bicuculline re-docking and loxapine and olanzapine docking, four runs were performed (referred to as "Sets of Results" in the Results and Discussion chapters). Inside each run, the three poses with the best Confidence score were selected. The only exception was the fourth bicuculline run, where Pose 4 was chosen instead of Pose 3 for its higher similarity with the experimental bicuculline belonging to the

6HUK structure.

- PLIP: for each ligand, the pose with the highest score is represented in the Results chapter. Data from the second and third top-ranked poses are included in the Supplementary materials chapter (Table 15).

4. Results

4.1 Results of the radioligand displacement assay experiments

For the radioligand displacement assays, only the pooled results data are shown in this subchapter. Two graphs are related to the experiments with compounds tested at 1 mM concentration (Figure 5) and two to the experiments with compounds tested at 100 µM concentration (Figure 6). Figure 5a and Figure 6a show the actual specific [^{3}H]-muscimol binding expressed in raw dpm. The X-axis indicates the different experimental conditions (100%, GABA, the compounds), while the Y-axis displays the radioactivity measured in the beta-counter (dpm). The height of the bar correlates with the measured radioligand amount. The two dotted lines represent the average values of the 100% and GABA conditions, respectively. The 100% line serves a reference to identify which drugs increased or decreased binding, and represents the condition with only [^{3}H]-muscimol bound to the receptors. The GABA line (bk, "background") represents the condition with a high GABA concentration, and thus the non-specific binding, or the fraction of binding insensitive to GABA. These references allow for a visual assessment of whether drugs alter the specific [^{3}H]-muscimol binding to $GABA_A$ receptors, with the space between the two dotted lines representing the total specific binding attributable to muscimol.

Figure 5b and Figure 6b illustrate the same data after normalisation, where the positive control is fixed at 100%. The normalised results will be the ones actually taken into account for drawing conclusions, as they reflect specific binding. Formula 3 found in the Materials and methods chapter was used to express each drug with respect to the 100% control condition of Figures 5a and 6a. In these graphs, the X-axis includes the tested drugs and their concentrations, while the Y-axis represents the percentage of specific [^{3}H]-muscimol binding compared to the control. The dotted line provides a clean, directly comparable overview of which drugs increased or decreased [^{3}H]-muscimol binding.

In all graphs of Figure 5 and Figure 6, each black dot represents the value measured in a single tube for that specific condition or drug. There were two experiments in triplicate at 1

mM and four experiments in triplicate at 100 μM for haloperidol and olanzapine, with loxapine used at 1 mM as the control, inside the second and the fourth assay. The height of the grey bars represents the mean of those points, while the black vertical line inside each grey bar indicates the standard deviation or error.

All graphs were made by the author of this thesis, using the GraphPad Prism 8 program, except where noted otherwise. Graphs for experimental results at 1 mM are firstly displayed (Figure 5).

a) b)

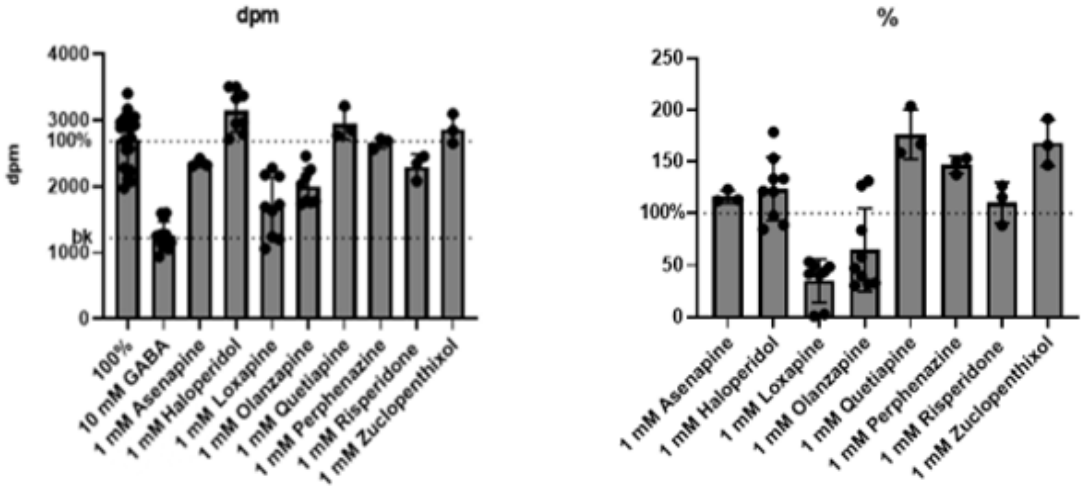

Figure 5. a) Raw data in dpm for the effect of 1 mM test compound on the binding of [^{3}H]-muscimol to $GABA_A$ receptors in hippocampal membranes. The 100% value is the mean of 24 data points. Non-specific binding (bk) was determined with 10 mM GABA, n = 12. For the test compounds, individual data points are displayed along with mean and Standard Deviation (SD). Dotted lines indicate 100% and blank mean values. For haloperidol, loxapine, and olanzapine, three experiments in triplicate are shown; for all the other ligands, one experiment in triplicate;
b) Data from panel a, normalised to the 100% value.

Looking at the normalised data (Figure 5b), it is possible to state that olanzapine was the only test compound capable of displacing [^{3}H]-muscimol.

Subsequently, the compounds were tested at 100 μM.

a) b)

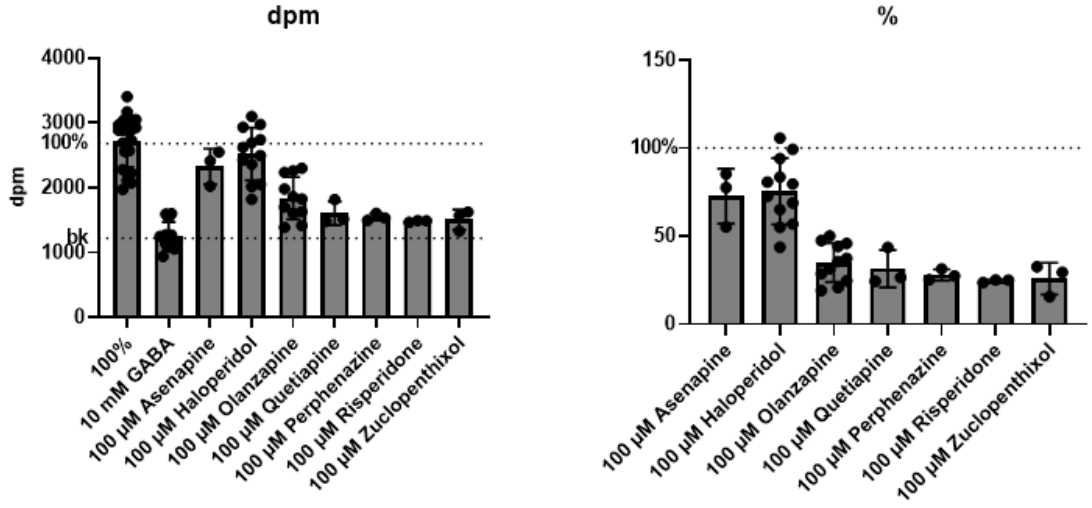

Figure 6. a) Raw data in dpm for the effect of 100 µM test compound on the binding of [^{3}H]-muscimol to $GABA_A$ receptors in hippocampal membranes. The 100% value is the mean of 24 data points. Non-specific binding (bk) was determined with 10 mM GABA, n = 12. For the test compounds, individual data points are displayed along with mean and Standard Deviation (SD). Dotted lines indicate 100% and blank mean values. For haloperidol and olanzapine, four experiments in triplicate are shown; for all the other ligands, one experiment in triplicate;
b) Data from panel a, normalised to the 100% value.

Figure 6b seems to suggest that most of the compounds displaced [^{3}H]-muscimol at 100 µM concentration. Due to some issues with the pipetting, where unexpectedly not all of the [^{3}H]-muscimol was actually used up, this pilot study was completed with two further assays performed by one of the researchers of the hosting laboratory, again with loxapine used as the control (Figure 7). The setup of Figure 7 is the same as Figure 5b and Figure 6b, and Figure 7 reflects the final results of the displacement study. Results from Figures 5 and 6 were not evaluated further.

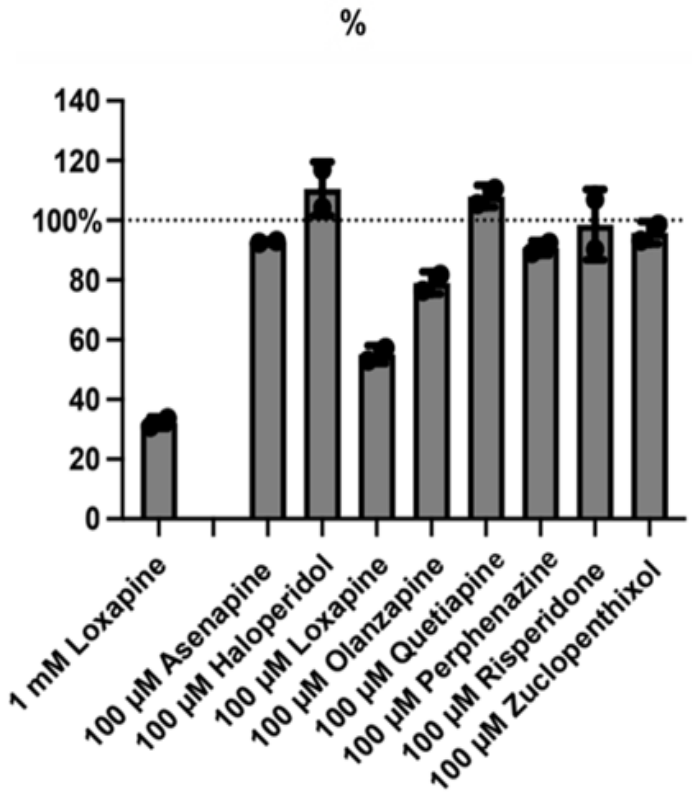

Figure 7. This graph was generated using the GraphPad Prism 8 software by one of the researchers of the hosting laboratory. It shows normalised data to the 100% value from two additional assays, which were performed in triplicate at 100 µM concentration of the compounds. 1 mM loxapine was used as the control again.

The complete study (Figure 7) showed much less scattered data, and confirmed olanzapine to be the compound that, together with the loxapine control, displaced muscimol. Only this complete study will be examined in the Discussion chapter, as the previous results are inconclusive. No further experiments at 1 mM were performed because it was of main interest to match the electrophysiological results.

In the following subchapter, the results of the computational analyses are presented.

4.2 Results of the computational analyses

4.2.1 Computational alignments

Using the published loxapine docking (Müller et al., 2024), all the test compounds were aligned with it using their pharmacophore features. Asenapine, olanzapine, quetiapine, and zuclopenthixol displayed the best alignment with loxapine among all the compounds. Consequently, these four alignments were visualised for this thesis with VMD, as shown in Figure 8.

a)

LOX-ASE aligned	LOX only	ASE only
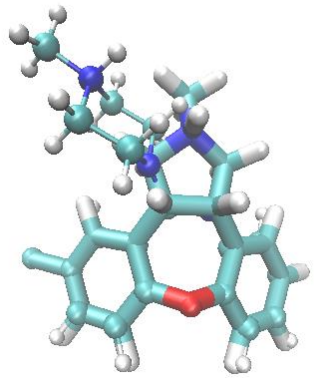	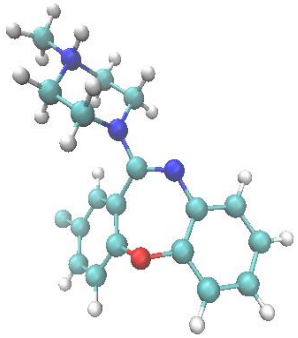	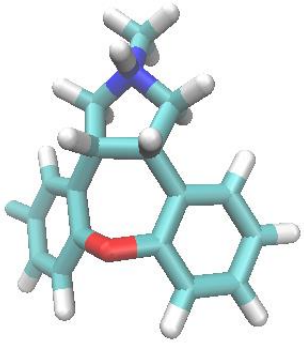

b)

LOX-OLA aligned	LOX only	OLA only
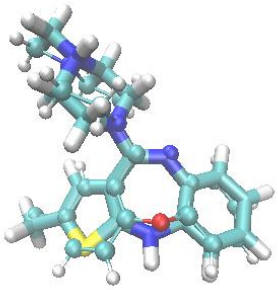	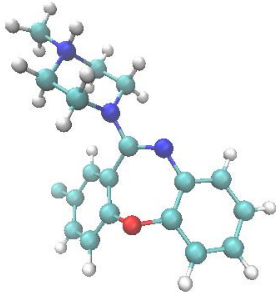	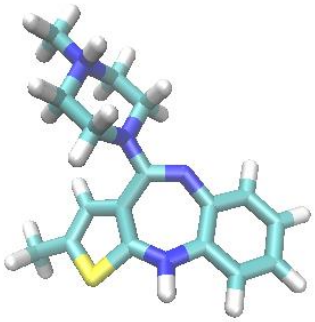

c)

LOX-QUE aligned	LOX only	QUE only
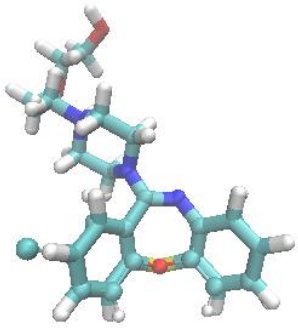	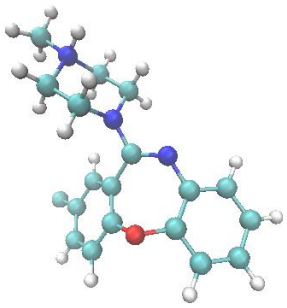	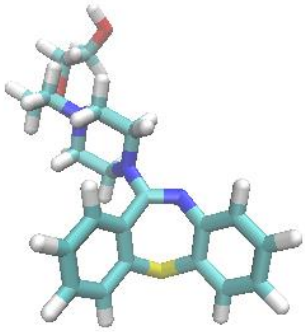

d)

LOX-ZUC aligned	LOX only	ZUC only
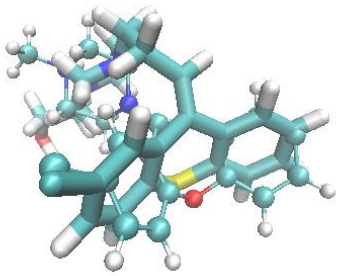	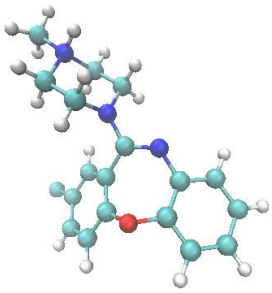	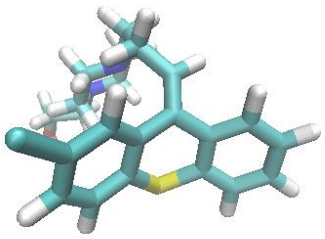

Figure 8. The alignment between loxapine and some of the tested antipsychotics is observed in the first column, while loxapine alone and the other antipsychotic alone are shown in the second and third columns, respectively. Loxapine is visualised as balls and sticks, while the other compounds are visualised as sticks. Carbon and chloride are cyan, hydrogen is white, nitrogen is blue, oxygen is red, and sulphur is yellow.
a) Loxapine aligned with asenapine, and their individual structures;
b) Loxapine aligned with olanzapine, and their individual structures;
c) Loxapine aligned with quetiapine, and their individual structures;
d) Loxapine aligned with zuclopenthixol, and their individual structures.

Olanzapine displayed the best shape match with loxapine, consistently following its volumetric profile and sharing highly similar pharmacophoric features. Conversely, among

the ligands showing high overlap, asenapine exhibited the largest volumetric difference. Being the smallest ligand tested, a significant portion of its structure deviated entirely from the volume occupied by loxapine. Quetiapine and zuclopenthixol showed a good overall fit – though not as close as olanzapine – due to their larger size relative to loxapine. Considering both these alignments and the results of the final displacement assay, olanzapine was the compound that behaved most similarly to loxapine. Therefore, only these two compounds were subsequently docked into the GABA binding site to avoid false positives, after bicuculline re-docking. In DiffDock, for all three ligands, the analysis of the collected results was based on visual inspection, not on calculations. All visualisations were made with VMD, except where indicated.

4.2.2 Computational re-docking and docking

Bicuculline re-docking was firstly performed to see whether DiffDock is able to find the experimental model and how it ranks it. This ligand represents the control compound since it is known that it binds to the GABA binding site, as stated in the Introduction. Figure 9 shows the poses obtained for this ligand and their correspondent Confidence score. If the score is greater than 0, the pose is considered high confidence; if it is between -1.5 and 0, the pose is considered moderate confidence; if it is below -1.5, the pose is considered low confidence. Dimers and not the entire protein were used, even for loxapine and olanzapine, to restrict the docking options that the DiffDock algorithm could give.

Ligand	Comparison image	Pose number	Confidence score
Bicuculline poses from Set 1 + experimental bicuculline (cyan)	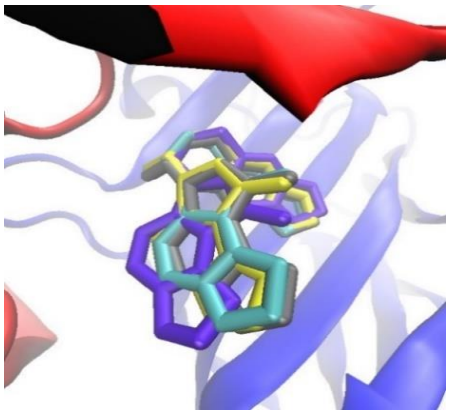	1 (grey), 2 (yellow), 3 (violet)	0.118 (pose 1), 0.004 (pose 2), -0.018 (pose 3)

Bicuculline poses from Set 2 + experimental bicuculline (cyan)	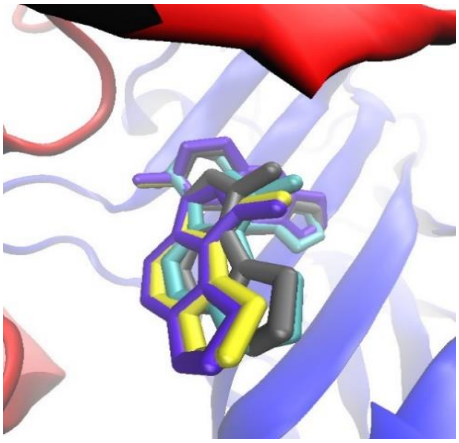	1 (grey), 2 (yellow), 3 (violet)	0.011 (pose 1), -0.025 (pose 2), -0.148 (pose 3)
Bicuculline poses from Set 3 + experimental bicuculline (cyan)	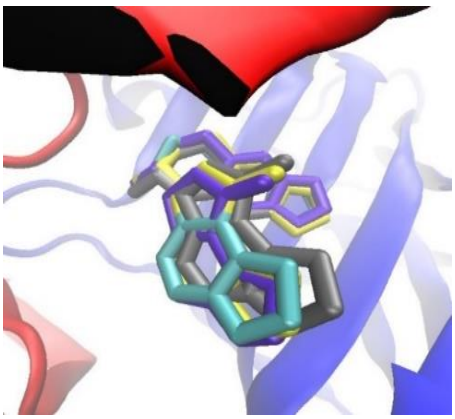	1 (grey), 2 (yellow), 3 (violet)	0.045 (pose 1), -0.122 (pose 2), -0.188 (pose 3)
Bicuculline poses from Set 4 + experimental bicuculline (cyan)	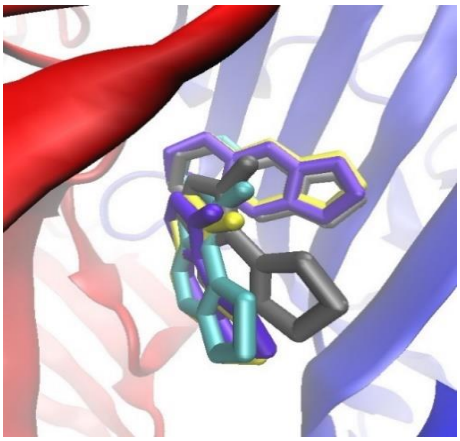	1 (grey), 2 (yellow), 4 (violet)	0.051 (pose 1), -0.415 (pose 2), -0.673 (pose 4)

Figure 9. Obtained bicuculline poses from each Set of Results compared among them and with the experimental bicuculline from 6HUK. Chain B (β3) is red and chain A (α1) is blue, while the experimental bicuculline is always cyan. For each pose, the Confidence score given by NVIDIA DiffDock is indicated. If the score is greater than 0, the pose is considered high confidence; if it is between -1.5 and 0, the pose is considered moderate confidence; if it is below -1.5, the pose is considered low confidence. Colour grey is always assigned to the pose with the highest score inside each Set, colour yellow to the pose with the second best score, and colour violet to the pose with the worst score (DiffDock Confidence scores explanation, 2024).

Bicuculline re-docking was performed at both the A/B (α1/β3) and D/E (α1/β3) sites. Ultimately, only the results of the A/B site were maintained, since bicuculline was better recognised and docked in the GABA binding site along this dimer, and A/B was used even for loxapine and olanzapine. Among the twelve generated poses, five achieved a positive score. Specifically, Pose 1 of Set 1 was identified as the highest-scoring pose, displaying a high degree of overlap with the experimental bicuculline structure (Figure 9). Conversely, seven out of twelve poses yielded a negative score, with Sets 2, 3, and 4 including two negative-scoring poses each (Figure 9). Consequently, Set 1 demonstrated the best overall performance, with two out of three poses scoring positively. Furthermore, despite having positive scores, Pose 1 of Set 3 and Pose 1 of Set 4 failed to correctly align with the experimental bicuculline (Figure 9), highlighting a limitation of DiffDock in accurately ranking these specific poses based solely on score. Nonetheless, all poses were inserted in this subchapter anyway to illustrate their structural trends compared to the experimental configuration.

Only the three highest-scoring poses were further analysed using PLIP. It is a computational tool that analyses three-dimensional structures to identify and map non-covalent chemical interactions between a protein and its ligand. Figure 10 and Table 6 illustrate the interaction profile with the receptor of the best-scoring pose (Pose 1 of Set 1) compared with the experimental bicuculline. The results of the two remaining poses are provided in the Supplementary materials chapter (Table 15).

a)

Pose number	Experimental bicuculline
Set of Results	Experimental bicuculline
PLIP image	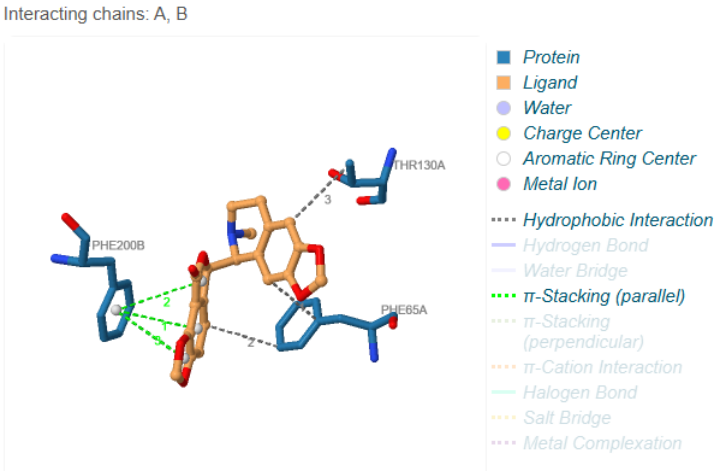

b)

Pose number	1
Set of Results	1
PLIP image	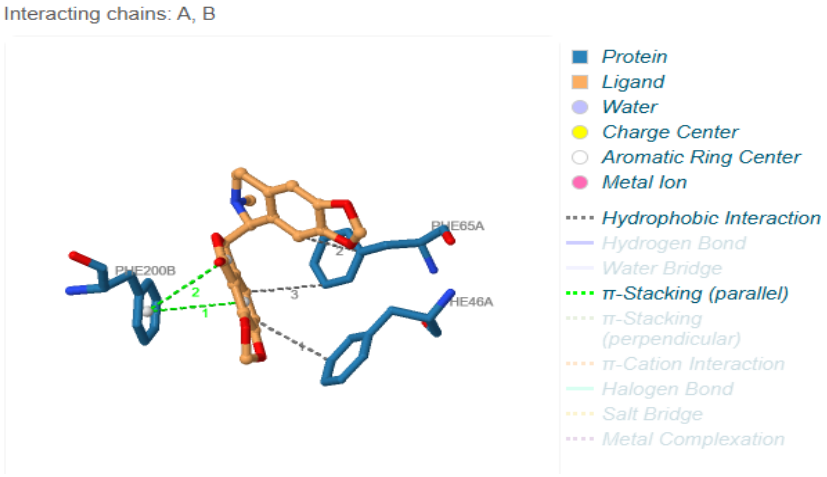

Figure 10. Results obtained with PLIP for the interaction profile of the experimental bicuculline (a) and the bicuculline pose with the best score (Pose 1 of Set 1) (b) with the receptor. The orange molecules are the ligands, whereas the dark blue amino acids belong to the receptor. The red portions in the ligands and receptor molecules are oxygen atoms, and the blue portions are nitrogen atoms. Concerning the representations of the interactions, Hydrophobic interactions are shown with grey

dotted lines and π-Stacking with green dotted lines.

		Experimental bicuculline		Pose 1 of Set 1	
Type of interaction	Index	Residue (amino acid + chain) (experimental bicuculline)	Distance (Å) (experimental bicuculline)	Residue (amino acid + chain) (obtained pose)	Distance (Å) (obtained pose)
Hydrophobic	1	65A (PHE)	3.66	46A (PHE)	3.90
Hydrophobic	2	65A (PHE)	3.97	65A (PHE)	3.68
Hydrophobic	3	130A (THR)	3.79	65A (PHE)	3.90
π-Stacking	1	200B (PHE)	3.80	200B (PHE)	3.98
π-Stacking	2	200B (PHE)	4.10	200B (PHE)	3.98
π-Stacking	3	200B (PHE)	3.97	-	-

Table 6. Table with the interactions listed and compared of the experimental bicuculline and bicuculline Pose 1 of Set 1 with the receptor. The Index column that follows the Type of interaction column corresponds to the bonds illustrated in Figure 10 (a and b) for each ligand, with the dotted or continuous lines. Concerning the Residue column, the number indicates the position of the amino acid in the correspondent chain, the letter soon after the number stands for the chain where the amino acid is located, and the three capital letters refer to the acronym of the amino acid. Then, the distance between the ligands and the amino acids of the receptor is reported in Ångström in the Distance column. The types of interactions are highlighted with different colours to make it easier to read.

PLIP analysis of Pose 1 of Set 1 revealed that its structure preserved five of the six interactions established by the experimental bicuculline with the receptor (Figure 10 and Table 6). Analysis of the second and third top-ranked poses showed that they displayed additional Hydrogen bonds or Salt Bridges alongside Hydrophobic interactions and π-Stacking bonds, while capturing fewer of the interactions present in the experimental model (Table 15, Supplementary materials chapter). Nevertheless, Hydrophobic interactions and π-Stacking bonds appear to form the primary binding core within the receptor pocket.

Since bicuculline re-docking resulted to be consistent, loxapine docking was subsequently carried out with four independent runs (Figure 11). For both loxapine and olanzapine, only poses with positive scores are presented.

Ligand	Comparison image	Pose number	Confidence score
Loxapine poses of Set of Results 1	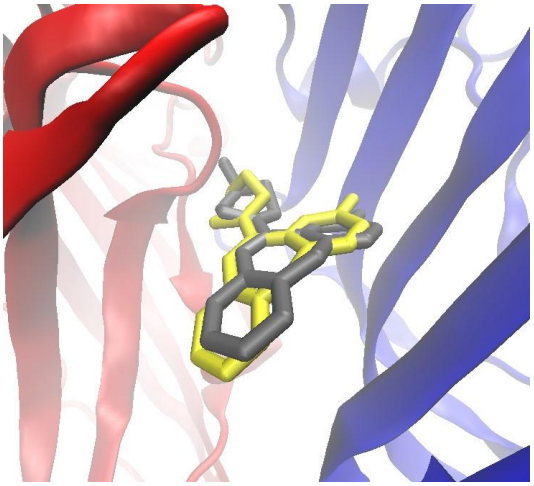	1 (grey), 2 (yellow)	0.441 (pose 1), 0.169 (pose 2)
Loxapine poses of Set of Results 2	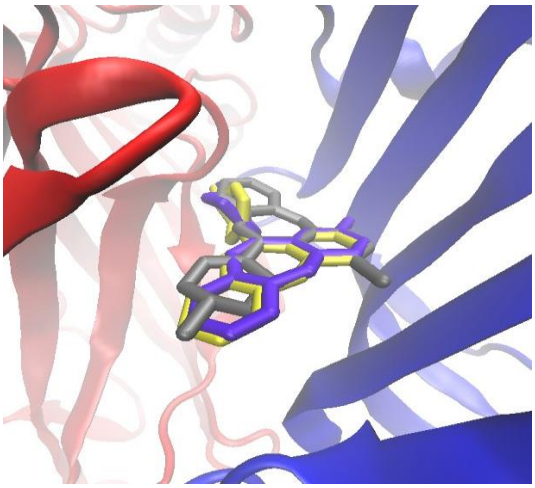	1 (grey), 2 (yellow), 3 (violet)	0.387 (pose 1), 0.371 (pose 2), 0.366 (pose 3)
Loxapine poses of Set of Results 3	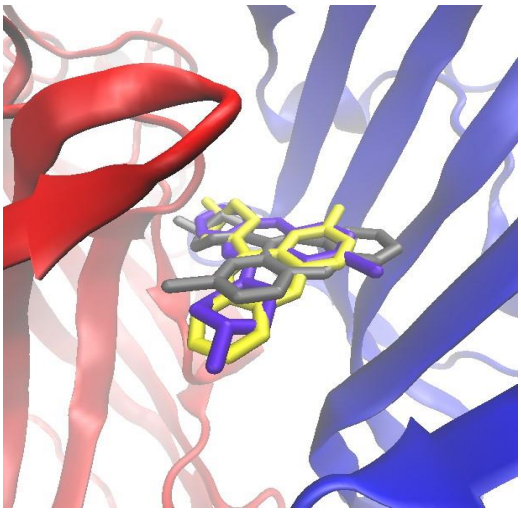	1 (grey), 2 (yellow), 3 (violet)	0.360 (pose 1), 0.129 (pose 2), 0.040 (pose 3)

Loxapine poses of Set of Results 4	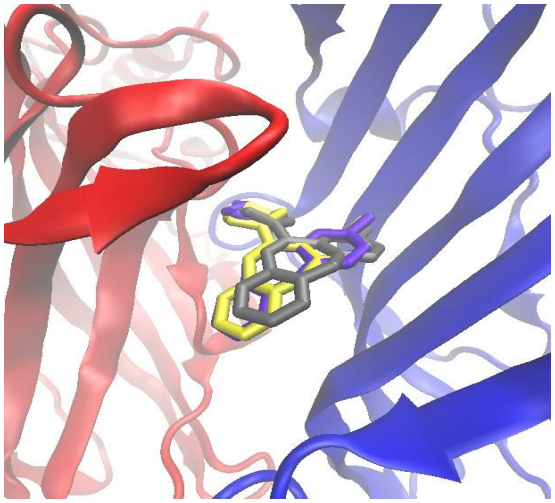	1 (grey), 2 (yellow), 3 (violet)	0.617 (pose 1), 0.195 (pose 2), 0.147 (pose 3)

Figure 11. Obtained loxapine poses with positive Confidence scores from each Set of Results. Chain B (β3) is red and chain A (α1) is blue. For each pose, the Confidence score given by NVIDIA DiffDock is indicated. If the score is greater than 0, the pose is considered high confidence; if it is between -1.5 and 0, the pose is considered moderate confidence; if it is below -1.5, the pose is considered low confidence. Colour grey is always assigned to the pose with the highest score inside each Set, colour yellow to the pose with the second best score, and colour violet to the pose with the worst score (DiffDock Confidence scores explanation, 2024).

Loxapine pose	Confidence score
Pose 1 of Set 1	0.441
Pose 2 of Set 1	0.169
Pose 3 of Set 1	-0.551
Pose 1 of Set 2	0.387
Pose 2 of Set 2	0.371
Pose 3 of Set 2	0.366
Pose 1 of Set 3	0.360
Pose 2 of Set 3	0.129
Pose 3 of Set 3	0.040
Pose 1 of Set 4	0.617
Pose 2 of Set 4	0.195
Pose 3 of Set 4	0.147

Table 7. List of all the loxapine poses obtained and their Confidence score. These latter are

highlighted in green if they are positive and resemble the published loxapine, and in blue if they are positive but do not resemble it.

Pose 1 of Set 4 displayed the highest score (Figure 11 and Table 7). Out of the twelve generated poses, only one yielded a negative score (Pose 3 of Set 1, Table 7), and was also located in a different binding pocket of the receptor. Among the remaining eleven poses, eight appeared to resemble the published loxapine structure, with two of them achieving the highest overall scores across all Sets. The remaining three poses displayed positive scores but adopted a different configuration compared to the published loxapine (Figure 11 and Table 7). Upon closer inspection, the loxapine molecules consistently exhibited varying degrees of conformational distortion. Observing distorted ligands with high Confidence scores was unexpected.

The analysis of loxapine continued with a visual comparison between the first pose of each Set and the loxapine structure reported by the Müller et al., 2024 paper.

a)

LOX Pose 1 of Set 4	Published LOX
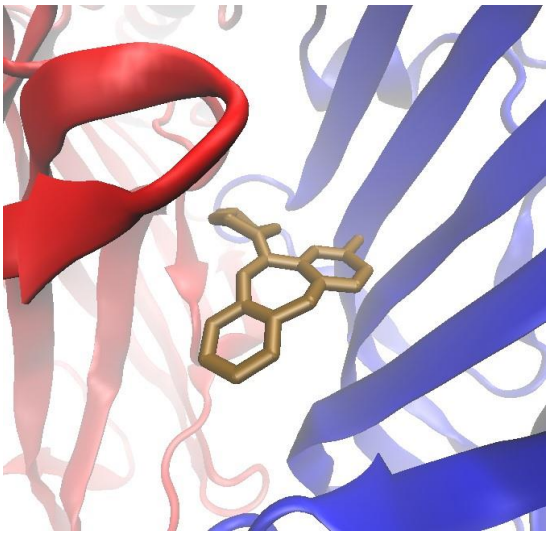	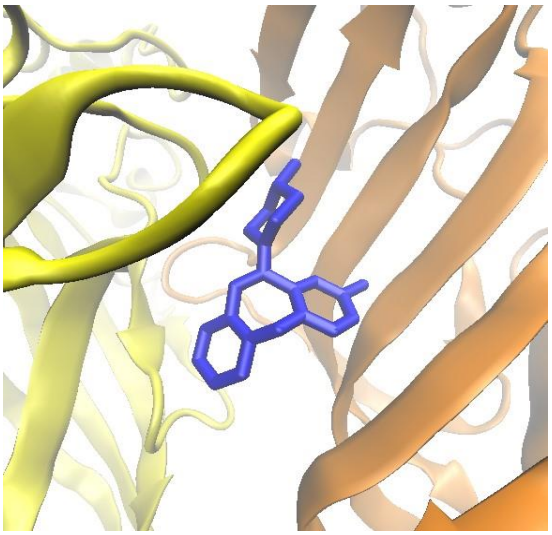

b)

LOX Pose 1 of Set 1	Published LOX
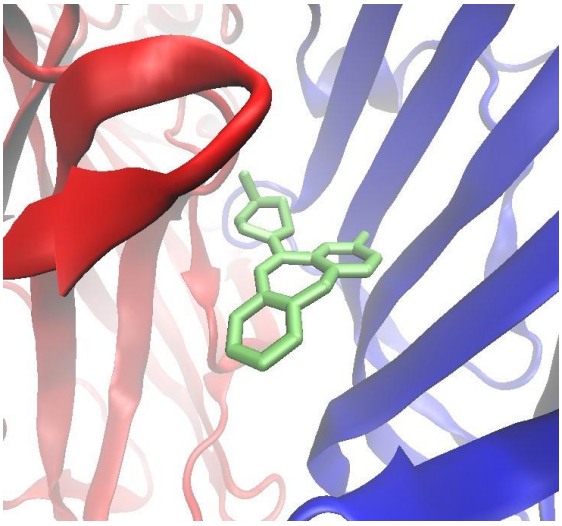	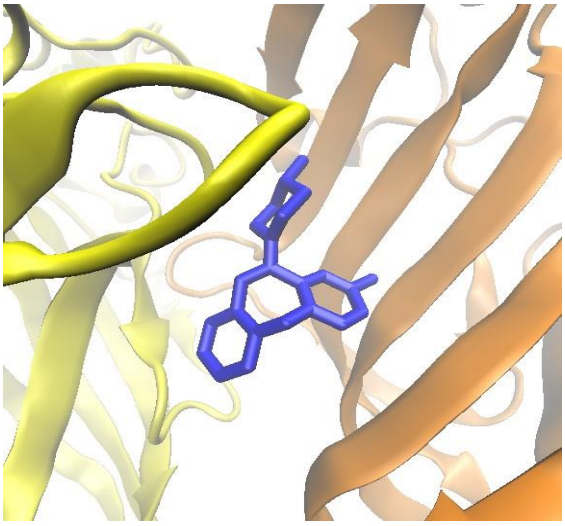

c)

LOX Pose 1 of Set 2	Published LOX
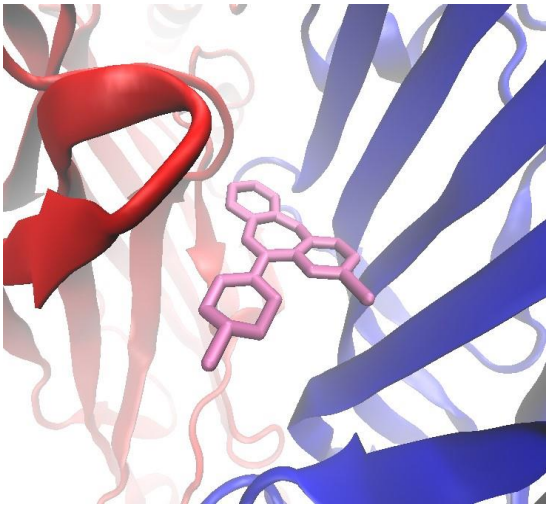	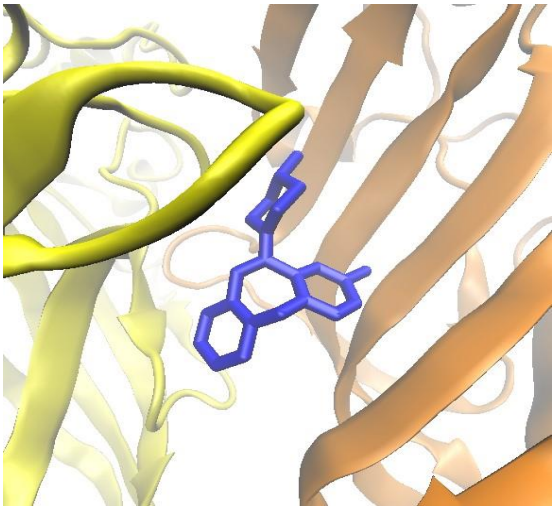

d)

LOX Pose 1 of Set 3	Published LOX
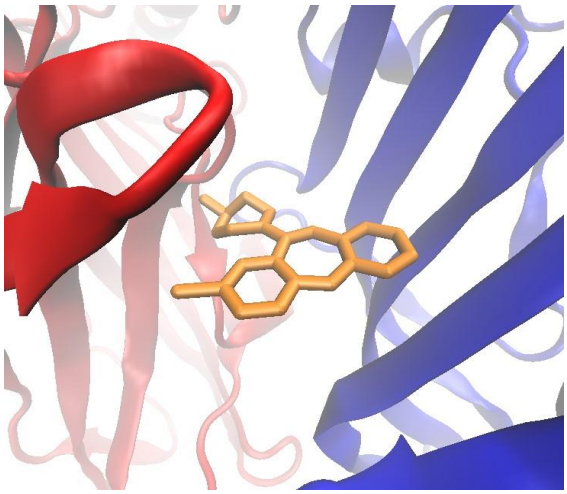	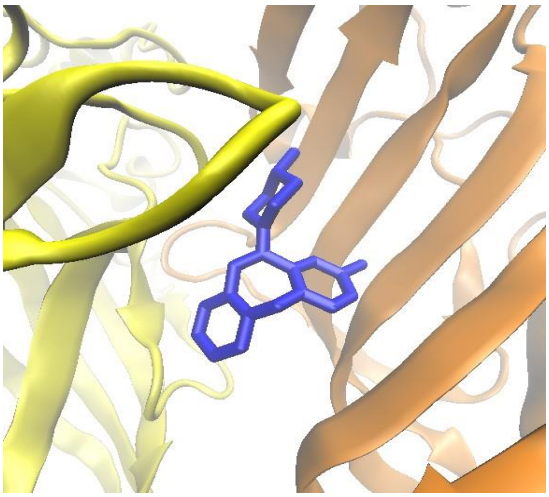

Figure 12. Comparison between the four loxapine poses (ordered by descending Confidence score) with the highest scores and the loxapine structure used in the Müller et al., 2024 paper, which was realised by one of the collaborators of the hosting laboratory. The ligands are visualised between chains D (α1, orange) and E (β3, yellow), as loxapine is located in the paper.
a) Loxapine Pose 1 of Set 4 and loxapine from the Müller et al., 2024 paper;
b) Loxapine Pose 1 of Set 1 and loxapine from the Müller et al., 2024 paper;
c) Loxapine Pose 1 of Set 2 and loxapine from the Müller et al., 2024 paper;
d) Loxapine Pose 1 of Set 3 and loxapine from the Müller et al., 2024 paper.

As shown in Figure 12, Pose 1 of Set 4 - the top-ranked pose – closely resembled the docked loxapine of the Müller et al., 2024 paper (Figure 12a), as Pose 1 of Set 1 did (Figure 12b). The only exception is the piperazine ring at the top, which adopts a different orientation. Conversely, Pose 1 of Set 3 (Figure 12d) is rotated 180° relative to the published model. Pose 1 of Set 2 did not resemble the published configuration (Figure 12c), even though it yielded the third highest score, emphasising that the Confidence score is not always predictive of pose classification. Therefore, two of the poses highlighted in blue in Table 7 differed both from the published structure and from each other. Additionally, all DiffDock poses appeared to be flatter than the structure reported in the paper.

Only the three highest-scoring poses were then analysed using PLIP, following the same procedure applied to bicuculline and later to olanzapine. Figure 13 and Table 8 illustrate

the interaction profile of the best-scoring pose (Pose 1 of Set 4), while the results of the remaining two poses are provided in the Supplementary materials chapter (Table 15).

Pose number	1
Set of Results	4
PLIP image	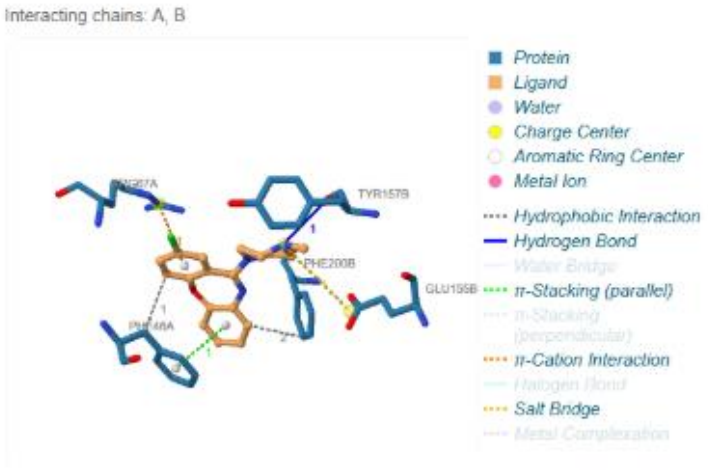

Figure 13. Results obtained with PLIP for the interaction profile of the loxapine pose with the best score (Pose 1 of Set 4) with the receptor. The orange molecule is the ligand, whereas the dark blue amino acids belong to the receptor. The red portions in the ligands and receptor molecules are oxygen atoms, the blue portions are nitrogen atoms, and the green portion is a chlorine atom. Concerning the representations of the interactions, Hydrophobic interactions are shown with grey dotted lines, the Hydrogen bond with a blue continuous line, the π-Stacking with a green dotted line, the π-Cation Interaction with an orange dotted line, and the Salt Bridge with a yellow dotted line.

Type of interaction	Index	Residue (amino acid + chain)	Distance (Å)
Hydrophobic	1	46A (PHE)	3.76
Hydrophobic	2	200B (PHE)	3.54
Hydrogen bond	1	157B (TYR)	3.20
π-Stacking	1	46A (PHE)	4.35
π-Cation Interaction	1	67A (ARG)	4.35
Salt Bridge	1	155B (GLU)	5.18

Table 8. Table with the interactions listed of loxapine Pose 1 of Set 4 with the receptor. The Index

column that follows the Type of interaction column corresponds to the bonds illustrated in Figure 13, with the dotted or continuous lines. In the Residue column, the number indicates the position of the amino acid in the correspondent chain, the letter soon after the number stands for the chain where the amino acid is located, and the three capital letters refer to the acronym of the amino acid. Then, the distance between the ligand and the amino acids of the receptor are reported in Ångström in the Distance column. The types of interactions are highlighted with different colours to make it easier to read.

PLIP analysis of the top-ranked pose revealed a diverse range of interaction types and engaging multiple amino acid residues (Figure 13 and Table 8), a structural diversity that was partially reduced in the second and third top-scoring poses (Table 15, Supplementary materials). However, Hydrophobic and π-Cation interactions were consistently retained across all poses (Figure 13, Table 8, and Table 15).

Thereafter, docking analyses were carried out for olanzapine.

Ligand	Image	Pose number	Confidence score
Olanzapine from Set of Results 1	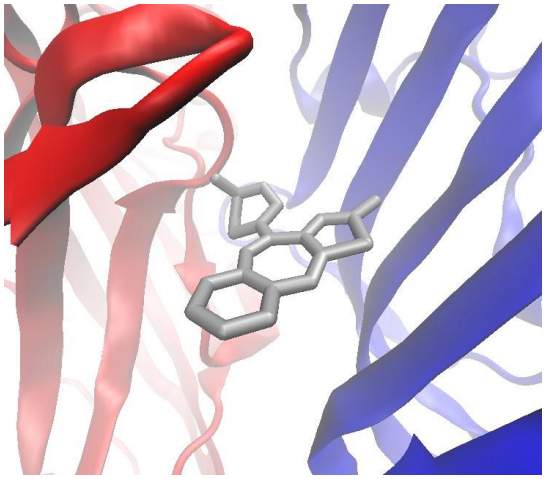	1	0.123

Olanzapine from Set of Results 4	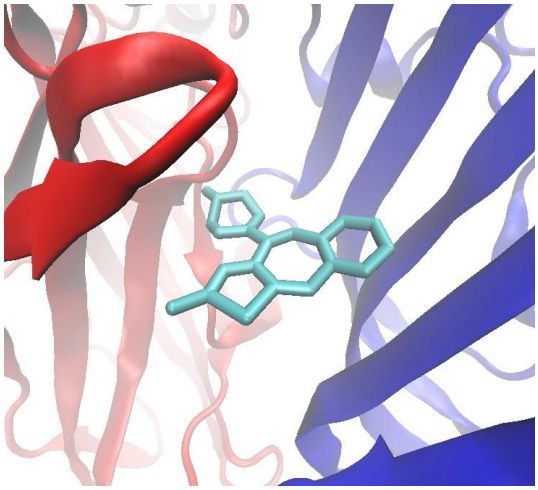	1	0.260
Olanzapine from Set of Results 4	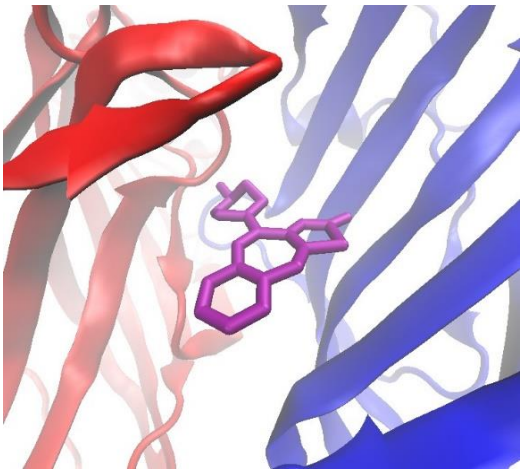	2	0.074

Figure 14. Obtained olanzapine poses with positive Confidence scores from each Set of Results. Chain B (β3) is red and chain A (α1) is blue. For each pose, the Confidence score given by NVIDIA DiffDock is indicated. If the score is greater than 0, the pose is considered high confidence; if it is between -1.5 and 0, the pose is considered moderate confidence; if it is below -1.5, the pose is considered low confidence (DiffDock Confidence score explanation, 2024).

Olanzapine pose	Confidence score
Pose 1 of Set 1	0.123
Pose 2 of Set 1	-0.168
Pose 3 of Set 1	-0.454
Pose 1 of Set 2	-0.135
Pose 2 of Set 2	-0.528
Pose 3 of Set 2	-0.697
Pose 1 of Set 3	-0.192
Pose 2 of Set 3	-0.656
Pose 3 of Set 3	-0.755
Pose 1 of Set 4	0.260
Pose 2 of Set 4	0.074
Pose 3 of Set 4	-0.137

Table 9. List of all the olanzapine poses obtained and their Confidence score. These latter are highlighted in red if they are positive.

DiffDock docking of olanzapine yielded the least favourable results among the tested compounds, as the platform generated several poses with negative scores. Only three out of the twelve obtained poses achieved a positive score (Figure 14 and Table 9). Except for Pose 2 of Set 1, all poses were bound within the pocket of interest. Nevertheless, Pose 2 of Set 1 did not get a strongly negative score, suggesting once again that the Confidence score is not consistently predictive for pose classification (Table 9). Among the three highest-scoring poses, the top-ranked pose did not resemble the configuration of the other two, which instead were similarly located in the pocket of interest. In this instance as well, DiffDock scoring did not appear particularly effective.

Concerning the interaction profile, only the three highest-scoring poses were then analysed using PLIP. Figure 15 and Table 10 illustrate the interactions formed by the best-scoring pose (Pose 1 of Set 4), while the results of the remaining two poses are provided in the Supplementary materials chapter (Table 15).

Pose number	1
Set of Results	4
PLIP image	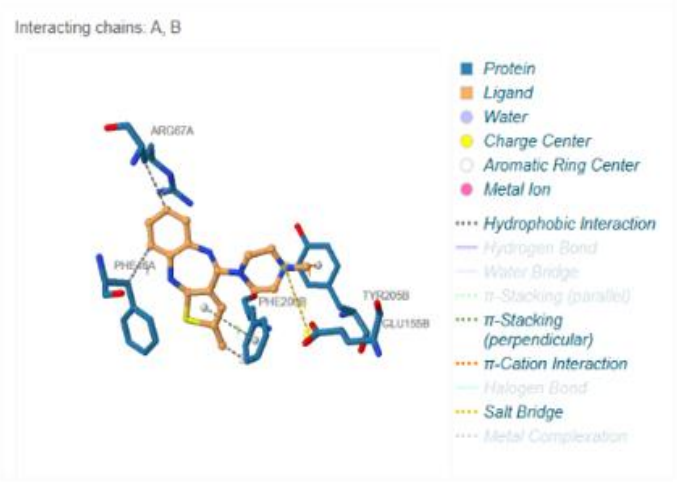

Figure 15. Results obtained with PLIP for the interaction profile of the olanzapine pose with the best score (Pose 1 of Set 4) with the receptor. The orange molecule is the ligand, whereas the dark blue amino acids belong to the receptor. The red portions in the ligands and receptor molecules are oxygen atoms, the blue portions are nitrogen atoms, and the yellow portion is a sulphur atom. Concerning the representation of the interactions, Hydrophobic interactions are shown with grey dotted lines, the π-Stacking with a green dotted line, the π-Cation Interaction with an orange dotted line, and the Salt Bridge with a yellow dotted line.

Type of interaction	Index	Residue (amino acid + chain)	Distance (Å)
Hydrophobic	1	46A (PHE)	3.60
Hydrophobic	2	67A (ARG)	3.29
Hydrophobic	3	200B (PHE)	1.91
π-Stacking	1	200B (PHE)	4.12
π-Cation Interaction	1	205B (TYR)	3.69
Salt Bridge	1	155B (GLU)	4.28

Table 10. Table with the interactions listed of olanzapine Pose 1 of Set 4 with the receptor. The Index column that follows the Type of interaction column corresponds to the bonds illustrated in Figure 15, with the dotted or continuous lines. Concerning the Residue column, the number indicates the position of the amino acid in the correspondent chain, the letter soon after the number stands for the chain where the amino acid is located, and the three capital letters refer to the acronym of the amino acid. Then, the distance between the ligands and the amino acids of the receptor are reported in Ångström in the Distance column. The types of interactions are highlighted with different colours to make it easier to read.

PLIP results revealed a diverse range of interactions between the top-ranked pose (Pose 1 of Set 4) and the receptor (Figure 15 and Table 10). Across the three highest-scoring poses, Hydrophobic interactions, π-Stacking bonds, and Salt Bridges emerged as the most prevalent interaction types (Figure 15, Table 10, and Table 15).

Finally, the top-ranked poses of loxapine and olanzapine were compared both to each other and to their true molecular structures.

a)

LOX Pose 1 of Set 4	OLA Pose 1 of Set 4
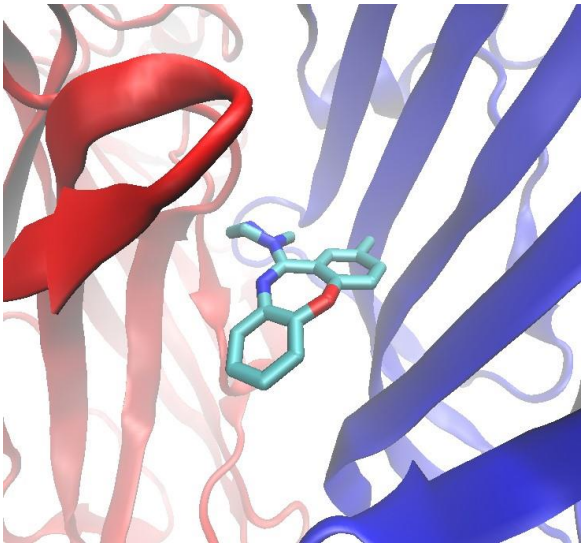	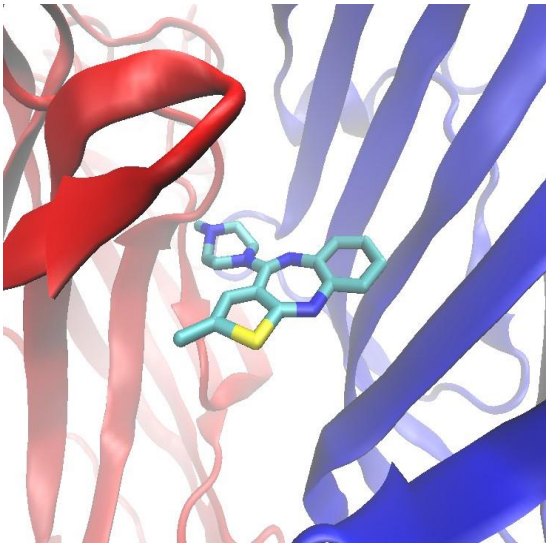

b)

LOX correct conformation	OLA correct conformation
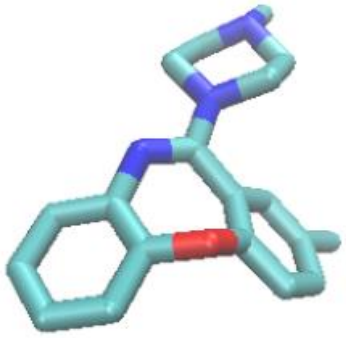	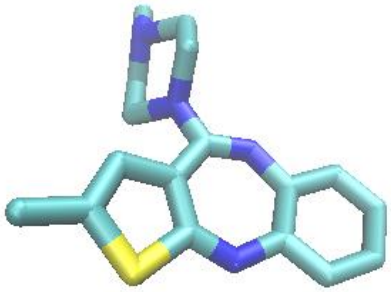

Figure 16. a) Best ranked pose for both loxapine and olanzapine. Chain B (β3) is red and chain A (α1) is blue. Carbon and chloride are cyan, nitrogen is blue, oxygen is red, and sulphur is yellow;
b) Loxapine and olanzapine correct conformation. Both structures were obtained from PubChem and are shown without hydrogens. Carbon and chloride are cyan, nitrogen is blue, oxygen is red, and sulphur is yellow.

Figure 16a compares the top-ranking poses of loxapine and olanzapine. Both of them successfully bound to the binding pocket of interest: loxapine seemed to resemble the published configuration, whereas olanzapine occupied the pocket similarly but was rotated by 180°. Furthermore, olanzapine appeared to be flatter than loxapine, highlighting distinct conformational and structural differences between the two, as shown in panel b). Looking at Figure 16b, it is evident that both poses did not preserve the structural characteristics of the original conformations, indicating that the algorithm struggles to maintain the correct configuration, with both DiffDock poses appearing markedly planar. To investigate this further, a specific angle was measured for one of the loxapine poses and compared with the reference structure (Müller et al., 2024), as illustrated in Figure 17.

LOX Pose 1 of Set 3	Published LOX
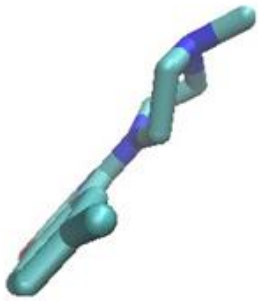	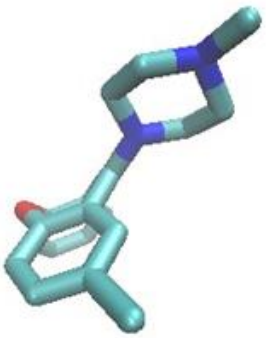
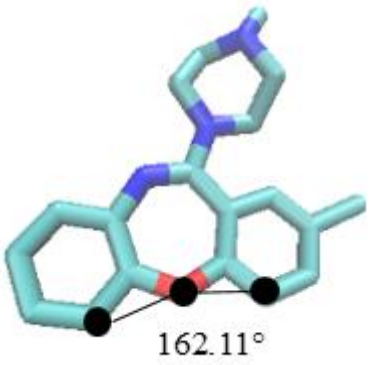	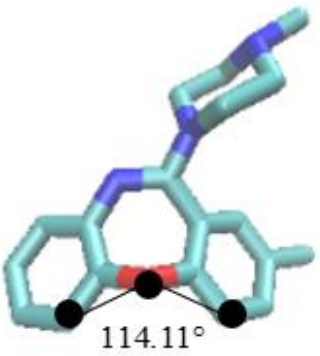

Figure 17. Loxapine Pose 1 of Set 3 and published loxapine visualised on VMD with two different orientations. The indicated, correspondent angles were measured always on VMD, and then they were resembled in PowerPoint 2013 to make them more visible. Their values are 162.11° for loxapine Pose 1 of Set 3 and 114.11° for the published loxapine. These structures are visualised without hydrogens. Carbon and chloride are cyan, nitrogen is blue, and oxygen is red.

Pose 1 of Set 3 was chosen for comparison with the experimental loxapine because it yielded the lowest score (Table 7) among the loxapine poses analysed in greater detail in Figure 12. It proved to be highly distorted compared to the experimental configuration. The black angle highlighted in Figure 17 corresponds in both structures, measuring 162.11° for loxapine Pose 1 of Set 3 and 114.11° for the published loxapine. This indicates that DiffDock distorted loxapine molecules.

5. Discussion

The aim of this study was to specifically test the orthosteric binding of selected antipsychotic medications on $GABA_A$ receptors. Electrophysiological studies were performed prior to the work presented in this thesis. Then, all antipsychotics were screened through radioligand displacement assay experiments. Finally, computational pharmacophore alignments were visualised and molecular docking analyses were executed as further support for the assay results.

5.1 Results of the radioligand displacement assays

The assays were performed to determine whether the compounds could bind to the GABA binding site and displace [^{3}H]-muscimol. At the same concentration used in the electrophysiological recordings, olanzapine was the only compound capable of displacing the radioligand (Figure 7). The minor differences between the 100% reference line and the bars of the other compounds did not represent a statistically significant reduction to state that they were able to displace [^{3}H]-muscimol.

Electrophysiological results (Table 3) show that all tested compounds reduced GABA-evoked currents. Overall, by combining the electrophysiology and the assay results, only olanzapine appeared to exhibit an orthosteric mechanism of action. All the other antipsychotics could behave as negative allosteric modulators or ion channel blockers.

5.2 Results of the computational analyses

The pharmacophore alignments (Figure 8) demonstrated the structural similarity between loxapine and olanzapine, indicating that they may share favourable interactions with the receptor within the GABA binding site. On the contrary, the alignments of the other three compounds with loxapine showed lower structural resemblance. Asenapine is smaller than loxapine, whereas quetiapine and zuclopenthixol are larger. These features could suggest

that a reduction in favourable interactions can lead to diminished binding affinity, while shape mismatch could prevent binding altogether due to steric clashes. Given their high structural similarity, only loxapine and olanzapine were selected for subsequent molecular docking analyses. The aim was to either support or question the published loxapine pose bound to the GABA binding site (Müller et al., 2024), as well as to investigate how olanzapine interacts within the orthosteric site and whether it adopts a binding mode comparable to loxapine.

In DiffDock, bicuculline re-docking initially provided confidence that DiffDock could be suitable for the analysed ligands, even though bicuculline poses did not obtain particularly high scores (Figure 9). Subsequent docking revealed surprisingly high scores for loxapine, despite its poses displaying variable configurations (Figure 11 and Table 7). However, the majority of these poses was similar to the published loxapine reported by the Müller et al., 2024 paper (Figure 11, Figure 12, and Table 7), prompting the question as to why bicuculline scores were lower in comparison. Conversely, olanzapine was the ligand that performed the worst, with only three out of twelve poses yielding positive scores. These three poses appeared similar to the published loxapine configuration (Figure 12, Figure 14, Table 9, and Figure 16a). Upon closer inspection, the DiffDock loxapine poses were structurally distorted. In particular, Pose 1 of Set 3 exhibited pronounced discrepancies relative to the published loxapine structure (Figure 17).

Nevertheless, all three ligands share the same binding site as well as Hydrophobic and π-Stacking interactions established with the receptor, as observed with PLIP (Figure 10, Table 6, Figure 13, Table 8, Figure 15, Table 10, and Table 15). These interaction types also correlate well with the biological properties, with minor variations regarding π-Stacking interactions, as outlined by Table 16 in the Supplementary materials chapter. Furthermore, no direct correlation appears to exist between the Confidence score and the number of interactions (Table 6, Table 8, Table 10, and Table 15). It could be possible that non-top-ranked poses adopt configurations that allow a greater number and diversity of interactions compared to the top-ranked pose. Overall, these results suggest that, despite structural distortions and ranking limitations, the three ligands may share a conserved binding pattern toward the receptor.

5.3 Final considerations, limitations, conclusion

A reduction in GABA-evoked currents was observed for all tested compounds, as summarised in Table 3. In hippocampal membranes, rich in α5 subunit, olanzapine was the only compound able to displace [^{3}H]-muscimol, suggesting that it is the sole novel orthosteric ligand identified in this study. The comparison between a recombinant system including only α5β3γ2 $GABA_A$ receptors, used in the electrophysiology, and an animal-derived system with a heterogeneous subunit composition, such as the hippocampal membranes used in the assays, represents a potential methodological limitation. The recombinant system was previously reported to exhibit high variability (Müller et al., 2024), complicating the interpretation of the results. Consequently, it was no longer used for this thesis.

Another biological issue is that $GABA_A$ receptors can combine multiple subunits. Although the α5 subunit is particularly abundant in the hippocampus, as already explained in the Introduction, radioligand binding assays only indicate whether the used concentration was able to displace no, some, or all of the muscimol in comparison to the control value with GABA. This does not make the researcher able to understand if a drug is selective for other subunits or some of their combinations. Furthermore, in the pilot assay experiments, pipetting and filtration accuracy problems could have influenced the results.

The experimental findings are quite supported by the pharmacophore alignments. The questions that were investigated with the docking are if it is possible to provide a structural hypothesis for olanzapine binding and if the previously published one for loxapine can be supported by using an AI-based docking program (Yu et al., 2023), evaluating the results with PLIP. In essence, the docking added support for the previous loxapine result, and suggests that olanzapine can bind as proposed by the pharmacophore model. However, serious limitations were encountered in the way DiffDock handles ligands. The platform seriously distorted both molecules, which deformations being more obvious for loxapine and more subtle for olanzapine. It can therefore generate physically implausible molecular structures (Buttenschoen et al., 2024). Furthermore, this platform performs blind docking on the entire protein rather than targeting a restricted pocket (Yu et al., 2023). This is why computational analyses were performed using dimers and not an entire protein. It is also very likely that it mispredicts key molecular properties - such as stereochemistry, bond lengths,

and steric interactions - leading to physically unrealistic predictions, as evidenced by the present results (Lee et al., 2025). The Confidence scores also appear to exhibit limitations, as evidenced by the paradoxically high scores assigned to the structurally distorted loxapine poses compared to the lower scores obtained by the structurally sound bicuculline poses. Therefore, the use of DiffDock in its current version cannot be recommended.

On the other hand, PLIP's first limitation pertains to its dependence on the coordinate quality of the input file: structural imperfections can lead to the generation of artifactual or false interactions by the platform. This issue is partially addressed by increasing the biological and ideal parameters of atomic distances of the interactions (Table 16, Supplementary materials). Moreover, despite not modifying molecular structures as DiffDock does, PLIP gives back exclusively favourable interactions, requiring complementary tools to detect unfavourable contacts. Finally, because cut-off distances and angle limits can be customised by the user, there is an inherent risk of introducing false positives or omitting real interactions (Schake et al., 2025; Salentin et al., 2015). Nevertheless, PLIP remains a valuable tool for the rapid, high-throughput profiling of non-covalent interactions.

In conclusion, despite the mentioned limitations, this type of work was useful to confirm what was found in the Bampali et al., 2022 and Müller et al., 2024 papers, and to perform pilot studies on other antipsychotics. Determining whether a drug acts as a competitive antagonist at a specific binding site is crucial for rational drug design and for assessing whether it potentiates or inhibits a given pharmacological effect. Further assays will be necessary to investigate the precise mechanisms of action of the tested antipsychotics in greater depth.
Computational docking of loxapine corroborated the configuration and binding mode reported by the Müller et al., 2024 paper, indicating that a new configuration does not need to be proposed. Furthermore, the docking suggested that olanzapine may adopt a comparable pose within the orthosteric GABA binding site. An additional contribution of this thesis was the use and evaluation of the DiffDock platform, which exhibited significant performance limitations. Future studies will be valuable to further explore the computational profile of olanzapine, confirm the behaviour of the remaining antipsychotics, and evaluate alternative docking platforms. Future developments aim to improve the predictive accuracy of this platform and the physical plausibility of conformations (Li et al., 2024).

6. List of abbreviations

6HUK — PDB code for CryoEM structure of human full-length α1β3γ2L $GABA_A$ receptor with bicuculline and megabody Mb38;

9G60 — PDB code for CryoEM structure of human ρ1 $GABA_A$ receptor in complex with muscimol and neurosteroid THDOC in the primed state;

AIFA — Agenzia Italiana del Farmaco;

ALA — alanine;

AMPA — α-amino-3-hydroxy-5-methyl-4-isoxazole-propionic acid;

ARG — arginine;

ASE — asenapine;

BBB — blood brain barrier;

Bbt — barbiturate;

bk — background line;

BZ — benzodiazepine;

C — concentration (molarity);

CA1 — Cornu Ammonis 1;

CA3 — Cornu Ammonis 3;

CCK — cholecystokinin;

ChB — channel blocker site;

CIAS — cognitive impairment associated with schizophrenia;

Ci/mmol — Curie per millimole;

Cl^- — chloride ion;

CNS — central nervous system;

COMT — catechol-O-methyltransferase gene;

cpm — counts per minute;

Cre — Causes recombination protein;

cryo-EM — cryo-electron microscopy;

CSF — cerebrospinal fluid;

D1Rs — D1 receptors;

D2Rs — D2 receptors;

DG — dentate gyrus;

DiffDock — Diffusion-based Molecular Docking;

DMSO — dimethyl sulfoxide;

dpm — disintegrations per minute;

dpm/fmol — disintegrations per minute per femtomole;

EC_{50} — Half-Maximal Effective Concentration;

ECD — extracellular domain;

EDTA — ethylenediaminetetraacetic acid;

E/I — excitation/inhibition;

Eto — etomidate;

FA — Fractional anisotropy;

FAERS — FDA Adverse Event Reporting System;

GABA — γ-aminobutyric acid;

$GABA_A$ — γ-aminobutyric acid type A receptor;

GAD67 — glutamate decarboxylase 67;

GAT-1 — GABA transporter type 1;

GF/B Filters — Glass Microfiber / Grade B filters;

GLU — glutamic acid/glutamate;

GRM3 — Glutamate Metabotropic Receptor 3;

GWAS — genome-wide association studies;

H2O — water;

HEK cells — Human Embryonic Kidney cells;

Hepes — 4-(2-hydroxyethyl)-1-piperazineethanesulfonic acid;

[^{3}H]-muscimol — tritiated muscimol;

ICD — intracellular domain;

IFG — inferior frontal gyrus;

IPSPs — inhibitory postsynaptic potentials;

LOX — loxapine;

m — mass;

M — molarity;

M1/M4 — type 1 and type 4 muscarinic acetylcholine receptors;

MFG — middle frontal gyrus;

mGluR — metabotropic glutamate receptor;

Milli-Q — Millipore Corporation Quantitative/Qualitative;

MW — molecular weight;

MWM — Morris Water Maze;

NAc — nucleus accumbens;

NaCl — sodium chloride;

NAMs — negative allosteric modulators;

NaOH — sodium hydroxide;

NMDA — N-methyl-D-aspartate;

NMDAR(s) — N-methyl-D-aspartate receptor(s);

OLA — olanzapine;

PAMs — positive allosteric modulators;

PCP — phencyclidine;

PDB — Protein Data Bank;

PDB ID — Protein Data Bank Identifier;

PET — positron emission tomography;

pH — potential of Hydrogen;

PHE — phenylalanine;

PLIP — Protein-Ligand Interaction Profiler;

PQ — pyrazoloquinolinones;

PRODH — proline dehydrogenase gene;

PV — parvalbumin;

QUE — quetiapine;

Roche — Complete Protease Inhibitor Tablette;

rpm — revolutions per minute;

SAMs — silent allosteric modulators;

SD — Standard Deviation;

SS34 — Superspeed 34 tubes;

SST — somatostatin;

TBI — traumatic brain injury;

TC50 — Tris-Calcium 50 mM buffer;

TC50/NaCl — Tris-Chloride 50 mM / Sodium Chloride;

TC500 — Tris-Calcium 500 mM buffer;

THR — threonine;

TM1 — transmembrane domain 1;

TM3 — transmembrane domain 3;

TM4 — transmembrane domain 4;

TMD — transmembrane domain;

Tris — Tris(hydroxymethyl)aminomethane;

Tris-Citrat — Tris(hydroxymethyl)aminomethane citrate;

TYR — tyrosine;

V — volume;

vHipp — ventral hippocampus;

VMD — Visual Molecular Dynamics;

VP — ventral pallidum;

VTA — ventral tegmental area;

ZDHHC8 — palmitoyl-transferase gene;

ZUC — zuclopenthixol.

7. References

1) Abi-Dargham A, Javitch JA, Slifstein M, Anticevic A, Calkins ME, Cho YT, Fonteneau C, Gil R, Girgis R, Gur RE, Gur RC, Grinband J, Kantrowitz J, Kohler C, Krystal J, Murray J, Ranganathan M, Santamauro N, Van Snellenberg J, Tamayo Z, Wolf D, Gray D, Lieberman J; TRANSCENDS Group. Dopamine D1R receptor stimulation as a mechanistic pro-cognitive target for schizophrenia. *Schizophr Bull*. 2022;48(1):199–210. doi:10.1093/schbul/sbab095.

2) Adamu MJ, Qiang L, Nyatega CO, Younis A, Kawuwa HB, Jabire AH, Saminu S. Unraveling the pathophysiology of schizophrenia: insights from structural magnetic resonance imaging studies. *Front Psychiatry*. 2023;14:1188603. doi:10.3389/fpsyt.2023.1188603.

3) Adell A. What value do NMDA receptor antagonist models of schizophrenia have for novel drug discovery? *Expert Opin Drug Discov*. 2025;20(11):1377–1385. doi:10.1080/17460441.2025.2562017.

4) Almulla AF, Al-Hakeim HK, Maes M. Schizophrenia phenomenology revisited: positive and negative symptoms are strongly related reflective manifestations of an underlying single trait indicating overall severity of schizophrenia. *CNS Spectr*. 2021;26(4):368–377. doi:10.1017/S1092852920001182.

5) An M, Jiang J. Comprehensive evaluation of flumazenil adverse reactions: insights from FAERS data and signal detection algorithms. *Medicine (Baltimore)*. 2025;104(10):e41721. doi:10.1097/MD.0000000000041721.

6) Bampali K, Koniuszewski F, Silva LL, Rehman S, Vogel FD, Seidel T, Scholze P, Zirpel F, Garon A, Langer T, Willeit M, Ernst M. Tricyclic antipsychotics and antidepressants can inhibit α5-containing GABAA receptors by two distinct mechanisms. *Br J Pharmacol*. 2022;179(14):3675–3692. doi:10.1111/bph.15807.

7) Bhandage AK, Hellgren C, Jin Z, Olafsson EB, Sundström-Poromaa I, Birnir B. Expression of GABA receptor subunits in peripheral blood mononuclear cells is gender dependent, altered in pregnancy and modified by mental health. *Acta Physiol*. 2015;213:575–585. doi:10.1111/apha.12440.

8) Brunelin J, Fecteau S, Suaud-Chagny MF. Abnormal striatal dopamine transmission in schizophrenia. *Curr Med Chem*. 2013;20(3):397–404. doi:10.2174/0929867311320030011.

9) Buttenschoen M, Morris GM, Deane CM. PoseBusters: AI-based docking methods fail to generate physically valid poses or generalise to novel sequences. *Chem Sci*. 2024;15(9):3130–3139. doi:10.1039/d3sc04185a.

10) Carbon M, Correll CU. Thinking and acting beyond the positive: the role of the cognitive and negative symptoms in schizophrenia. *CNS Spectr*. 2014;19(S1):35–53. doi:10.1017/S1092852914000601.

11) Corso G, Stark H, Jing B, Barzilay R, Jaakkola T. DiffDock: diffusion steps, twists and turns for molecular docking. *ICLR Conf Proc*. 2023.

12) Cowgill J, Fan C, Haloi N, et al. Structure and dynamics of differential ligand binding in the human ρ-type GABAA receptor. *Neuron*. 2023;111(21):3450–3464.e5. doi:10.1016/j.neuron.2023.08.006.

13) Crestani F, Keist R, Fritschy JM, Benke D, Vogt K, Prut L, Blüthmann H, Möhler H, Rudolph U. Trace fear conditioning involves hippocampal α5-GABAA receptors. *Proc Natl Acad Sci U S A*. 2002;99(13):8980–8985. doi:10.1073/pnas.142288699.

14) Cutting GR, Lu L, O'Hara BF, Kasch LM, Montrose-Rafizadeh C, Donovan DM, Shimada S, Antonarakis SE, Guggino WB, Uhl GR, et al. Cloning of the gamma-aminobutyric acid (GABA) rho 1 cDNA: a GABA receptor subunit highly expressed in the retina. *Proc Natl Acad Sci U S A*. 1991;88(7):2673–2677. doi:10.1073/pnas.88.7.2673.

15) Daher F, Fukushima CT, Ingebretsen EA, Bidlack JM, Atack JR, Popa MO, Fogaça MV. Negative allosteric modulation of α5-GABAA receptors engages dynamic cortical glutamatergic and GABAergic mechanisms underlying adaptive behavior in mice. *bioRxiv*. 2026. doi:10.64898/2026.01.15.699507.

16) Donegan JJ, Boley AM, Yamaguchi J, et al. Modulation of extrasynaptic GABAA α5 receptors in the ventral hippocampus normalizes physiological and behavioral deficits in a circuit-specific manner. *Nat Commun*. 2019;10:2819. doi:10.1038/s41467-019-10800-1.

17) Fadgyas-Stanculete M, Capatina OO. Glutamate-based therapeutic strategies for schizophrenia: emerging approaches beyond dopamine. *Int J Mol Sci*. 2025;26(9):4331. doi:10.3390/ijms26094331.

18) Farrant M, Nusser Z. Variations on an inhibitory theme: phasic and tonic activation of GABAA receptors. *Nat Rev Neurosci*. 2005;6:215–229. doi:10.1038/nrn1625.

19) Ferreira de Freitas R, Schapira M. A systematic analysis of atomic protein-ligand interactions in the PDB. *Medchemcomm*. 2017;8(10):1970–1981. doi:10.1039/c7md00381a.

20) Fluyau D, Revadigar N, Manobianco BE. Challenges of the pharmacological management of benzodiazepine withdrawal, dependence, and discontinuation. *Ther Adv Psychopharmacol*. 2018;8(5):147–168. doi:10.1177/2045125317753340.

21) Frankle WG, Paris J, Himes M, Mason NS, Mathis CA, Narendran R. Amphetamine-induced striatal dopamine release measured with an agonist radiotracer in schizophrenia. *Biol Psychiatry*. 2018;83(8):707–714. doi:10.1016/j.biopsych.2017.11.032.

22) Fritschy JM, Weinmann O, Wenzel A, Benke D. Synapse-specific localization of NMDA and GABAA receptor subunits revealed by antigen-retrieval immunohistochemistry. *J Comp Neurol*. 1998;390(2):194–210.

23) Fujihara K. Beyond the γ-aminobutyric acid hypothesis of schizophrenia. *Front Cell Neurosci*. 2023;17:1161608. doi:10.3389/fncel.2023.1161608.

24) Gaulton TG, Wunsch H, Gaskins LJ, Leonard CE, Hennessy S, Ashburn M, Brensinger C, Newcomb C, Wijeysundera D, Bateman BT, Bethell J, Neuman MD. Preoperative sedative hypnotic medication use and adverse postoperative outcomes. *Ann Surg*. 2021;274(2):e108–e114. doi:10.1097/SLA.0000000000003556.

25) Gill KM, Grace AA. The role of α5 GABAA receptor agonists in the treatment of cognitive deficits in schizophrenia. *Curr Pharm Des*. 2014;20(31):5069–5076. doi:10.2174/1381612819666131216114612.

26) Glahn DC, Laird AR, Ellison-Wright I, Thelen SM, Robinson JL, Lancaster JL, Bullmore E, Fox PT. Meta-analysis of gray matter anomalies in schizophrenia: application of anatomic likelihood estimation and network analysis. *Biol Psychiatry*. 2008;64(9):774–781. doi:10.1016/j.biopsych.2008.03.031.

27) Gonzalez-Burgos G, Lewis DA. NMDA receptor hypofunction, parvalbumin-positive neurons, and cortical gamma oscillations in schizophrenia. *Schizophr Bull*. 2012;38(5):950–957. doi:10.1093/schbul/sbs010.

28) Hashimoto T, Arion D, Unger T, et al. Alterations in GABA-related transcriptome in the dorsolateral prefrontal cortex of subjects with schizophrenia. *Mol Psychiatry*. 2008;13:147–161. doi:10.1038/sj.mp.4002011.

29) Hedblom E, Kirkness EF. A novel class of GABAA receptor subunit in tissues of the reproductive system. *J Biol Chem*. 1997;272(24):15346–15350. doi:10.1074/jbc.272.24.15346.

30) Hipp JF, Knoflach F, Comley R, Ballard TM, Honer M, Trube G, Gasser R, Prinssen E, Wallace TL, Rothfuss A, Knust H, Lennon-Chrimes S, Derks M, Bentley D, Squassante L, Nave S, Nöldeke J, Wandel C, Thomas AW, Hernandez MC. Basmisanil, a highly selective GABAA-α5 negative allosteric modulator: preclinical pharmacology and demonstration of functional target engagement in man. *Sci Rep*. 2021;11(1):7700. doi:10.1038/s41598-021-87307-7.

31) Howes OD, Kapur S. The dopamine hypothesis of schizophrenia: version III—the final common pathway. *Schizophr Bull*. 2009;35(3):549–562. doi:10.1093/schbul/sbp006.

32) Howes OD, Shatalina E. Integrating the neurodevelopmental and dopamine hypotheses of schizophrenia and the role of cortical excitation–inhibition balance. *Biol Psychiatry*. 2022;92(6):501–513. doi:10.1016/j.biopsych.2022.06.017.

33) Humphrey W, Dalke A, Schulten K. VMD: visual molecular dynamics. *J Mol Graph*. 1996;14(1):33–38. doi:10.1016/0263-7855(96)00018-5.

34) Iorio MT, Vogel FD, Koniuszewski F, Scholze P, Rehman S, Simeone X, Schnürch M, Mihovilovic MD, Ernst M. GABAA receptor ligands often interact with binding sites in the transmembrane domain and in the extracellular domain—can the promiscuity code be cracked? *Int J Mol Sci*. 2020;21:334. doi:10.3390/ijms21010334.

35) Jacob TC. Neurobiology and therapeutic potential of α5-GABA type A receptors. *Front Mol Neurosci*. 2019;12:179. doi:10.3389/fnmol.2019.00179.

36) Jiménez-García B, Teixeira JMC, Trellet M, Rodrigues JPGLM, Bonvin AMJJ. PDB-tools web: a user-friendly interface for the manipulation of PDB files. *Proteins*. 2021;89(3):330–335. doi:10.1002/prot.26018.

37) Johnston GA. Advantages of an antagonist: bicuculline and other GABA antagonists. *Br J Pharmacol*. 2013;169(2):328–336. doi:10.1111/bph.12127.

38) Johnston GAR. Muscimol as an ionotropic GABA receptor agonist. *Neurochem Res*. 2014;39:1942–1947. doi:10.1007/s11064-014-1245-y.

39) Karam CS, Ballon JS, Bivens NM, Freyberg Z, Girgis RR, Lizardi-Ortiz JE, Markx S, Lieberman JA, Javitch JA. Signaling pathways in schizophrenia: emerging targets and therapeutic strategies. *Trends Pharmacol Sci*. 2010;31(8):381–390. doi:10.1016/j.tips.2010.05.004.

40) Kelly S, Jahanshad N, Zalesky A, et al. Widespread white matter microstructural differences in schizophrenia across 4322 individuals: results from the ENIGMA Schizophrenia DTI Working Group. *Mol Psychiatry*. 2018;23(5):1261–1269. doi:10.1038/mp.2017.170.

41) Kerti-Szigeti K, Nusser Z. Similar GABAA receptor subunit composition in somatic and axon initial segment synapses of hippocampal pyramidal cells. *Elife*. 2016;5:e18426. doi:10.7554/eLife.18426.

42) Kim JJ, Hibbs RE. Direct structural insights into GABAA receptor pharmacology. *Trends Biochem Sci*. 2021;46(6):502–517. doi:10.1016/j.tibs.2021.01.011.

43) Lee J, Nguyen CH, Mamitsuka H. Beyond rigid docking: deep learning approaches for fully flexible protein–ligand interactions. *Brief Bioinform*. 2025;26(5):bbaf454. doi:10.1093/bib/bbaf454.

44) Leucht S, Priller J, Davis JM. Antipsychotic drugs: a concise review of history, classification, indications, mechanism, efficacy, side effects, dosing, and clinical application. *Am J Psychiatry*. 2024;181(10). doi:10.1176/appi.ajp.20240738.

45) Lewis DA, Curley AA, Glausier JR, Volk DW. Cortical parvalbumin interneurons and cognitive dysfunction in schizophrenia. *Trends Neurosci*. 2012;35(1):57–67. doi:10.1016/j.tins.2011.10.004.

46) Li M, Szabo A, Rosenberg HC. Evaluation of native GABAA receptors containing an α5 subunit. *Eur J Pharmacol*. 2001;413(1):63–72. doi:10.1016/S0014-2999(01)00751-8.

47) Li Y, Lin H, Yang H, et al. Synergistic application of molecular docking and machine learning for improved binding pose. *Natl Sci Open*. 2024;3(2):2024-03-08. doi:10.1360/nso/20230058.

48) Liemburg E, Sibeijn-Kuiper A, Bais L, et al. Prefrontal NAA and Glx levels in different stages of psychotic disorders: a 3T 1H-MRS study. *Sci Rep*. 2016;6:21873. doi:10.1038/srep21873.

49) Liu S, Xu L, Guan F, et al. Cryo-EM structure of the human α5β3 GABAA receptor. *Cell Res*. 2018;28:958–961. doi:10.1038/s41422-018-0077-8.

50) Marques TR, Ashok AH, Angelescu I, et al. GABAA receptor differences in schizophrenia: a positron emission tomography study using [11C]Ro154513. *Mol Psychiatry*. 2021;26:2616–2625. doi:10.1038/s41380-020-0711-y.

51) Marty A, Llano I. Excitatory effects of GABA in established brain networks. *Trends Neurosci*. 2005;28(6):284–289. doi:10.1016/j.tins.2005.04.003.

52) Masiulis S, Desai R, Uchański T, et al. GABAA receptor signalling mechanisms revealed by structural pharmacology. *Nature*. 2019;565:454–459. doi:10.1038/s41586-018-0832-5.

53) McGrath JJ, Eyles DW, Pedersen CB, et al. Neonatal vitamin D status and risk of schizophrenia: a population-based case-control study. *Arch Gen Psychiatry*. 2010;67(9):889–894. doi:10.1001/archgenpsychiatry.2010.110.

54) Mihaylov DB, Malinauskas T, Aricescu AR. Cryo-EM structure of the α1β3 GABAA receptor in complex with GABA and Mb25 in the long-lived symmetric desensitised state. *Forthcoming*.

55) Mohamad FH, Mohamad Jamali M, Che Has A. Structure–function studies of GABAA receptors and related computer-aided studies. *J Mol Neurosci*. 2023;73:804–817. doi:10.1007/s12031-023-02158-3.

56) Mortensen M, Smart TG. Extrasynaptic αβ subunit GABAA receptors on rat hippocampal pyramidal neurons. *J Physiol*. 2006;577:841–856. doi:10.1113/jphysiol.2006.117952.

57) Moya NA, Yun S, Fleps SW, et al. The effect of selective nigrostriatal dopamine excess on behaviors linked to the cognitive and negative symptoms of schizophrenia. *Neuropsychopharmacol*. 2023;48:690–699. doi:10.1038/s41386-022-01492-1.

58) Müller V, Ernst M, Baykuchkarova A, Koniuszewski F, Bampali K, Seidel T, Scholze P. Probes for the heterogeneity of muscimol binding sites in rat brain. *Front Pharmacol*. 2024;15:1368527. doi:10.3389/fphar.2024.1368527.

59) Ochalski PG, Fellows-Mayle W, Hsieh LB, et al. Flumazenil administration attenuates cognitive impairment in immature rats after controlled cortical impact. *J Neurotrauma*. 2010;27(3):647–651. doi:10.1089/neu.2009.1142.

60) Okubo R, Okada M, Motomura E. Dysfunction of the NMDA receptor in the pathophysiology of schizophrenia and/or the pathomechanisms of treatment-resistant schizophrenia. *Biomolecules*. 2024;14(9):1128. doi:10.3390/biom14091128.

61) Pirker S, Schwarzer C, Wieselthaler A, Sieghart W, Sperk G. GABAA receptors: immunocytochemical distribution of 13 subunits in the adult rat brain. *Neuroscience*. 2000;101(4):815–850. doi:10.1016/S0306-4522(00)00442-5.

62) Pistis M, Belelli D, McGurk K, Peters JA, Lambert JJ. Complementary regulation of anaesthetic activation of human (α6β3γ2L) and *Drosophila* (RDL) GABAA receptors by a single amino acid residue. *J Physiol*. 1999;515(Pt 1):3–18. doi:10.1111/j.1469-7793.1999.003ad.x.

63) Purcell S, Moran J, Fromer M, et al. A polygenic burden of rare disruptive mutations in schizophrenia. *Nature*. 2014;506:185–190. doi:10.1038/nature12975.

64) Puthenkalam R, Hieckel M, Simeone X, Suwattanasophon C, Feldbauer RV, Ecker GF, Ernst M. Structural studies of GABAA receptor binding sites: which experimental structure tells us what? *Front Mol Neurosci*. 2016;9:44. doi:10.3389/fnmol.2016.00044.

65) Ramerstorfer J, Furtmüller R, Sarto-Jackson I, Varagic Z, Sieghart W, Ernst M. The GABAA receptor α+β- interface: a novel target for subtype-selective drugs. *J Neurosci*. 2011;31(3):870–877. doi:10.1523/JNEUROSCI.5012-10.2011.

66) Rivera-Illanes D, Recabarren-Gajardo G. Classics in chemical neuroscience: muscimol. *ACS Chem Neurosci*. 2024;15(18):3257–3269. doi:10.1021/acschemneuro.4c00304.

67) Rosas-Arellano A, Estrada-Mondragón A, Martínez-Torres A, Reyes-Haro D. GABAA-ρ receptors in the CNS: their functional, pharmacological, and structural properties in neurons and astroglia. *Neuroglia*. 2023;4(4):239–252. doi:10.3390/neuroglia4040017.

68) Roth FC, Draguhn A. GABA metabolism and transport: effects on synaptic efficacy. *Neural Plast*. 2012;2012:805830. doi:10.1155/2012/805830.

69) Rudolph U, Knoflach F. Beyond classical benzodiazepines: novel therapeutic potential of GABAA receptor subtypes. *Nat Rev Drug Discov*. 2011;10(9):685–697. doi:10.1038/nrd3502.

70) Salentin S, Schreiber S, Haupt VJ, Adasme MF, Schroeder M. PLIP: fully automated protein-ligand interaction profiler. *Nucleic Acids Res*. 2015;43(W1):W443–W447. doi:10.1093/nar/gkv315.

71) Sallard E, Letourneur D, Legendre P. Electrophysiology of ionotropic GABA receptors. *Cell Mol Life Sci*. 2021;78:5341–5370. doi:10.1007/s00018-021-03846-2.

72) Samaha AN, Seeman P, Stewart J, Rajabi H, Kapur S. "Breakthrough" dopamine supersensitivity during ongoing antipsychotic treatment leads to treatment failure over time. *J Neurosci*. 2007;27(11):2979–2986. doi:10.1523/JNEUROSCI.5416-06.2007.

73) Sanabria E, Cuenca RE, Esteso MÁ, Maldonado M. Benzodiazepines: their use either as essential medicines or as toxic substances. *Toxics*. 2021;9(2):25. doi:10.3390/toxics9020025.

74) Schake P, Bolz SN, Linnemann K, Schroeder M. PLIP 2025: introducing protein–protein interactions to the protein–ligand interaction profiler. *Nucleic Acids Res*. 2025;53(W1):W463–W465. doi:10.1093/nar/gkaf361.

75) Sente A, Desai R, Naydenova K, et al. Differential assembly diversifies GABAA receptor structures and signalling. *Nature*. 2022;604(7904):190–194. doi:10.1038/s41586-022-04517-3.

76) Sequeira A, Shen K, Gottlieb A, et al. Human brain transcriptome analysis finds region- and subject-specific expression signatures of GABAAR subunits. *Commun Biol*. 2019;2:153. doi:10.1038/s42003-019-0413-7.

77) Shenton ME, Dickey CC, Frumin M, McCarley RW. A review of MRI findings in schizophrenia. *Schizophr Res*. 2001;49(1-2):1–52. doi:10.1016/S0920-9964(01)00163-3.

78) Sieghart W, Fuchs K, Tretter V, Ebert V, Jechlinger M, Höger H, Adamiker D. Structure and subunit composition of GABAA receptors. *Neurochem Int*. 1999;34(5):379–385. doi:10.1016/S0197-0186(99)00045-5.

79) Sigel E, Ernst M. The benzodiazepine binding sites of GABAA receptors. *Trends Pharmacol Sci*. 2018;39(7):659–671. doi:10.1016/j.tips.2018.03.006.

80) Singh A. Xanomeline and trospium: a potential fixed drug combination for schizophrenia—a brief review of current data. *Innov Clin Neurosci*. 2022;19(10–12):43–47.

81) Skene NG, Bryois J, Bakken TE, Breen G, Crowley JJ, Gaspar HA, Giusti-Rodriguez P, Hodge RD, Miller JA, Muñoz-Manchado AB, O'Donovan MC, Owen MJ, Pardiñas AF, Ryge J, Walters JTR, Linnarsson S, Lein ES; Major Depressive Disorder Working Group of the Psychiatric Genomics Consortium; Sullivan PF, Hjerling-Leffler J. Genetic identification of brain cell types underlying schizophrenia. *Nat Genet*. 2018;50(6):825–833. doi:10.1038/s41588-018-0129-5.

82) Sohal VS. Neurobiology of schizophrenia. *Curr Opin Neurobiol*. 2024;84:102820. doi:10.1016/j.conb.2023.102820.

83) Sperk G, Schwarzer C, Tsunashima K, Fuchs K, Sieghart W. GABAA receptor subunits in the rat hippocampus I: immunocytochemical distribution of 13 subunits. *Neuroscience*. 1997;80(4):987–1000. doi:10.1016/S0306-4522(97)00146-2.

84) Spivey WH, Roberts JR, Derlet RW. A clinical trial of escalating doses of flumazenil for reversal of suspected benzodiazepine overdose in the emergency department. *Ann Emerg Med*. 1993;22(12):1813–1821. doi:10.1016/S0196-0644(05)80407-X.

85) Squarcione C, Torti MC, Di Fabio F, Biondi M. 22q11 deletion syndrome: a review of the neuropsychiatric features and their neurobiological basis. *Neuropsychiatr Dis Treat*. 2013;9:1873–1884. doi:10.2147/NDT.S52188.

86) Stefanits H, Milenkovic I, Mahr N, et al. GABAA receptor subunits in the human amygdala and hippocampus: immunohistochemical distribution of 7 subunits. *J Comp Neurol*. 2018;526:324–348. doi:10.1002/cne.24337.

87) Sun C, Zhu H, Clark S, Gouaux E. Cryo-EM structures reveal native GABAA receptor assemblies and pharmacology. *Nature*. 2023;622(7981):195–201. doi:10.1038/s41586-023-06556-w.

88) Sur C, Quirk K, Dewar D, Atack J, McKernan R. Rat and human hippocampal α5-subunit-containing γ-aminobutyric acid A receptors have α5β3γ2 pharmacological characteristics. *Mol Pharmacol*. 1998;54(5):928–933. doi:10.1124/mol.54.5.928.

89) Thompson SM. Modulators of GABAA receptor-mediated inhibition in the treatment of neuropsychiatric disorders: past, present, and future. *Neuropsychopharmacol*. 2024;49:83–95. doi:10.1038/s41386-023-01728-8.

90) Tiihonen J, Tanskanen A, Solmi M, Rubio JM, Correll CU, Kane JM, Taipale H. Continuous dopamine D2 receptor blockade and long-term outcome in first-episode schizophrenia. *Am J Psychiatry*. 2025;182(4):341–348. doi:10.1176/appi.ajp.20240321.

91) Topchiy I, Mohbat J, Folorunso OO, Wang Z, Lazcano-Etchebarne C, Engin E. GABA system as the cause and effect in early development. *Neurosci Biobehav Rev*. 2024;161:105651. doi:10.1016/j.neubiorev.2024.105651.

92) Treviño M, Guerra-Crespo M, Padilla-Godínez FJ, Soto-Rojas LO, Manjarrez E, Ortega-Robles E, Rodríguez-de-Ita J, Arias-Carrión O. Decoding the structural and functional diversity of GABAA receptors: from ensemble logic to therapeutic opportunities. *Front Pharmacol*. 2025;16:1697905. doi:10.3389/fphar.2025.1697905.

93) Uliana DL, Popa MO, Paradowski M, Elvers KT, Hanley M, Baldwin A, Atack JR, Grace AA. Novel positive allosteric modulators of α5 subunit-containing GABAA receptors (α5-GABAARs) reverse the hyperdopaminergic state in a neurodevelopmental model of schizophrenia. *Schizophr Res*. 2026;291:27–36. doi:10.1016/j.schres.2026.02.010.

94) Umbricht D, Abt M, Derks M, et al. A phase 2b multicenter study to evaluate basmisanil as an adjunctive treatment in patients with cognitive impairment associated with schizophrenia. *J Clin Psychiatry*. 2026;87(2):25m16022.

95) Vallat B, Rose Y, Piehl DW, et al. RCSB Protein Data Bank: delivering integrative structures alongside experimental structures and computed structure models. *Nucleic Acids Res*. 2026;54(D1):D489–D498. doi:10.1093/nar/gkaf1187.

96) Vega Alanis BA, Iorio MT, Silva LL, Bampali K, Ernst M, Schnürch M, Mihovilovic MD. Allosteric GABAA receptor modulators: a review on the most recent heterocyclic chemotypes and their synthetic accessibility. *Molecules*. 2020;25(4):999. doi:10.3390/molecules25040999.

97) Vélez-Fort M, Audinat E, Angulo MC. Central role of GABA in neuron–glia interactions. *Neuroscientist*. 2012;18(3):237–250. doi:10.1177/1073858411403317.

98) Wang Y, Zhang Y, Li W, et al. GABAA receptor π forms channels that stimulate ERK through a G-protein-dependent pathway. *Mol Cell*. 2025;85(1):166–176.e5. doi:10.1016/j.molcel.2024.11.016.

99) Wójciak P, Rybakowski J. Clinical picture, pathogenesis and psychometric assessment of negative symptoms of schizophrenia. *Psychiatr Pol*. 2018;52(2):185–197. doi:10.12740/PP/70610.

100) Xu MY, Wong AHC. GABAergic inhibitory neurons as therapeutic targets for cognitive impairment in schizophrenia. *Acta Pharmacol Sin*. 2018;39(5):733–753. doi:10.1038/aps.2017.172.

101) Yu Y, Shuqi L, Gao Z, Zheng H, Ke G. Do deep learning models really outperform traditional approaches in molecular docking? *arXiv*. 2023. doi:10.48550/arXiv.2302.07134.

102) Zhan N, Sham PC, So HC, Lui SSY. The genetic basis of onset age in schizophrenia: evidence and models. *Front Genet*. 2023;14:1163361. doi:10.3389/fgene.2023.1163361.

103) Zhao Z, Li X, Xie Y, et al. Resolving the heterogeneity of dopamine subsystem dysfunction in schizophrenia: a PET meta-analysis. *Schizophr*. 2025;11:139. doi:10.1038/s41537-025-00684-0.

104) Zhou J, Noviello CM, Teng J, et al. Resolving native GABAA receptor structures from the human brain. *Nature*. 2025;638:562–568. doi:10.1038/s41586-024-08454-1.

105) Zhu S, Sridhar A, Teng J, Howard RJ, Lindahl E, Hibbs RE. Structural and dynamic mechanisms of GABAA receptor modulators with opposing activities. *Nat Commun*. 2022;13:4582. doi:10.1038/s41467-022-32212-4.

AIFA: https://www.aifa.gov.it/documents/20142/3159201/AIFA_Rapporto_OsMed_2024.pdf

ATC/DDD Index 2026: https://atcddd.fhi.no/atc_ddd_index/

BioGRID: https://thebiogrid.org/

DiffDock: https://build.nvidia.com/mit/diffdock

DiffDock Confidence scores explanation, 2024: https://www.bv-brc.org/docs/tutorial/docking/docking.html

DrugCentral: https://drugcentral.org/

Fisher Scientific: https://www.fishersci.com/us/en/home.html

GraphPad Radioactivity Calculator: https://www.graphpad.com/quickcalcs/radcalcform/

PDB: https://www.rcsb.org/

PDB-Tools: https://wenmr.science.uu.nl/pdbtools/submit

PLIP: https://plip-tool.biotec.tu-dresden.de/plip-web/plip/index

PLIP source configuration file: https://github.com/pharmai/plip/blob/master/plip/basic/config.py

PubChem: https://pubchem.ncbi.nlm.nih.gov/

ScienceCodons: https://sciencecodons.com/tools/sdf-to-mol2-converter/

SciMiner: https://sciminer.tech/utility/tool/Merge-Protein-And-Ligand

Sigma-Aldrich: https://www.sigmaaldrich.com/AT/de?srsltid=AfmBOooVnHGolEi1fveH19J4t855Q38E79hPtQ3C30EIOnfhSUD39rlw

Sophion report, 2024:
https://sophion.com/app/uploads/2024/09/Investigating-antipsychotic-compound-interactions_AR_Public40433-1.pdf

8. Supplementary materials

Nr	Final concentration	Membrane	TC50/ NaCl	100 mM GABA	DMSO	Drug	3H Musc. 100 nM
1	100 %	320 µL	40 µL	-	4 µL	-	40 µL
2	10 mM GABA		-	40 µL	4 µL	-	
3	1 mM Asenapine		40 µL	-	-	4 µL (100 mM)	
4	1 mM Haloperidol		40 µL	-	-	4 µL (100 mM)	
5	1 mM Loxapine		40 µL	-	-	4 µL (100 mM)	
6	1 mM Olanzapine		40 µL	-	-	4 µL (100 mM)	
7	1 mM Quetiapine		40 µL	-	-	4 µL (100 mM)	
8	1 mM Perphenazine		40 µL	-	-	4 µL (100 mM)	
9	1 mM Risperidone		40 µL	-	-	4 µL (100 mM)	
10	1 mM Zuclopenthixol		40 µL	-	-	4 µL (100 mM)	
11	100 %		40 µL	-	4 µL	-	

Table 11. Pipetting scheme of the first assay.

Nr	Final concentration	Membrane	TC50/ NaCl	100 mM GABA	DMSO	Drug	3H Musc. 100 nM
1	100 %	320 µL	40 µL	-	4 µL	-	40 µL
2	10 mM GABA		-	40 µL	4 µL	-	
3	1 mM Loxapine		40 µL	-	-	4 µL (100 mM)	
4	1 mM Haloperidol		40 µL	-	-	4 µL (100 mM)	
5	100 µM Haloperidol		40 µL	-	-	4 µL (10 mM)	
6	1 mM Olanzapine		40 µL	-	-	4 µL (100 mM)	
7	100 µM Olanzapine		40 µL	-	-	4 µL (10 mM)	
8	100 %		40 µL	-	4 µL	-	

Table 12. Pipetting scheme of the second assay.

Nr	Final concentration	Membrane	TC50/ NaCl	100 mM GABA	DMSO	Drug	3H Musc. 100 nM
1	100 %	320 µL	40 µL	-	4 µL	-	40 µL
2	10 mM GABA		-	40 µL	4 µL	-	
3	100 µM Asenapine		40 µL	-	-	4 µL (10 mM)	
4	100 µM Haloperidol		40 µL	-	-	4 µL (10 mM)	
5	100 µM Olanzapine		40 µL	-	-	4 µL (10 mM)	
6	100 µM Quetiapine		40 µL	-	-	4 µL (10 mM)	
7	100 µM Perphenazine		40 µL	-	-	4 µL (10 mM)	
8	100 µM Risperidone		40 µL	-	-	4 µL (10 mM)	
9	100 µM Zuclopenthixol		40 µL	-	-	4 µL (10 mM)	
10	100 %		40 µL	-	4 µL	-	

Table 13. Pipetting scheme of the third assay.

Nr	Final concentration	Membrane	TC50/ NaCl	100 mM GABA	DMSO	Drug	3H Musc. 100 nM
1	100 %	320 µL	40 µL	-	4 µL	-	40 µL
2	10 mM GABA		-	40 µL	4 µL	-	
3	1 mM Haloperidol		40 µL	-	-	4 µL (100 mM)	
4	100 µM Haloperidol		40 µL	-	-	4 µL (10 mM #1)	
5	100 µM Haloperidol		40 µL	-	-	4 µL (10 mM #2)	
6	1 mM Olanzapine		40 µL	-	-	4 µL (100 mM)	
7	100 µM Olanzapine		40 µL	-	-	4 µL (10 mM #1)	
8	100 µM Olanzapine		40 µL	-	-	4 µL (10 mM #2)	
9	1 mM Loxapine		40 µL	-	-	4 µL (100 mM)	
10	100 %		40 µL	-	4 µL	-	

Table 14. Pipetting scheme of the fourth assay.

Ligand	Type of interaction	Residue (amino acid + chain)	Distance (Å)
Bicuculline Pose 1 of Set 3	Hydrophobic	46A (PHE)	3.58
	Hydrophobic	65A (PHE)	3.71
	π-Stacking	200B (PHE)	3.95
	π-Stacking	200B (PHE)	3.99
	Salt Bridge	155B (GLU)	5.44
Bicuculline Pose 1 of Set 4	Hydrophobic	65A (PHE)	3.85
	Hydrogen bond	201B (ALA)	3.32
	Hydrogen bond	202B (THR)	3.06
	π-Stacking	46A (PHE)	4.72
	π-Stacking	200B (PHE)	4.12

	π-Stacking	200B (PHE)	4.03
	Salt Bridge	155B (GLU)	5.22
Loxapine Pose 1 of Set 1	Hydrophobic	46A (PHE)	3.95
	Hydrophobic	65A (PHE)	3.78
	Hydrophobic	200B (PHE)	3.51
	π-Stacking	46A (PHE)	4.49
	π-Cation Interaction	157B (TYR)	4.91
Loxapine Pose 1 of Set 2	Hydrophobic	65A (PHE)	3.25
	Hydrophobic	67A (ARG)	3.73
	Hydrophobic	205B (TYR)	3.84
	π-Cation Interaction	67A (ARG)	4.30
Olanzapine Pose 1 of Set 1	Hydrophobic	67A (ARG)	3.29
	Hydrophobic	130A (THR)	3.79
	Hydrogen bond	157B (TYR)	2.65
	π-Stacking	46A (PHE)	4.71
	π-Stacking	200B (PHE)	3.98
	Salt Bridge	155B (GLU)	5.10
Olanzapine Pose 2 of Set 4	Hydrophobic	67A (ARG)	3.48
	Hydrophobic	200B (PHE)	3.23
	π-Stacking	46A (PHE)	4.18
	π-Cation Interaction	205B (TYR)	4.76
	Salt Bridge	155B (GLU)	4.96

Table 15. Results obtained with PLIP for the second and third top-ranked poses for each ligand (bicuculline, loxapine, and olanzapine). The types of interactions obtained between the poses and the receptor are listed. Concerning the Residue column, the number indicates the position of the amino acid in the correspondent chain, the letter soon after the number stands for the chain where the amino acid is located, and the three capital letters refer to the acronym of the amino acid. Then, the distance between the ligands and the amino acids of the receptor are reported in Ångström in the Distance column. The types of interactions are highlighted with different colours to make it easier to read.

Type of interaction	Empirical statistical limit (PDB) (Å)	PLIP maximum threshold (Å)
Hydrophobic	≤ 4.0	4.0
Hydrogen bond	≤ 3.9	4.1
π-Stacking	≤ 4.0	5.5
π-Cation interaction	≤ 4.0	6.0
Salt Bridge	≤ 4.0	5.5

Table 16. For each type of interaction found in PLIP, both biological and PLIP distances between the atoms that take part in the interactions themselves are indicated. Biological distances in the second column refer to what can be documented in PDB. This data is located in the Ferreira de Freitas & Schapira, 2017, paper (table S2 of the Supplementary materials to be seen inside the paper). Distances of the same interactions assigned by PLIP are positioned in the third column (PLIP source configuration file).